UCSF
UC San Francisco Previously Published Works

Title

Caloric restriction disrupts the microbiota and colonization resistance

Permalink

https://escholarship.org/uc/item/0gf7764k

Journal

Nature, 595(7866)

ISSN

0028-0836

Authors

von Schwartzenberg, Reiner Jumpertz
Bisanz, Jordan E
Lyalina, Svetlana
et al.

Publication Date

2021-07-08

DOI

10.1038/s41586-021-03663-4

Peer reviewed

Article

Caloric restriction disrupts the microbiota and colonization resistance

Check for updates

Reiner Jumpertz von Schwartzenberg[1,2,3,13], Jordan E. Bisanz[4,13], Svetlana Lyalina[5], Peter Spanogiannopoulos[4], Qi Yan Ang[4], Jingwei Cai[6], Sophia Dickmann[1], Marie Friedrich[1], Su-Yang Liu[7], Stephanie L. Collins[6], Danielle Ingebrigtsen[8], Steve Miller[8], Jessie A. Turnbaugh[4], Andrew D. Patterson[6], Katherine S. Pollard[5,9,10,11,12], Knut Mai[1,2], Joachim Spranger[1,2,3,14 ✉] & Peter J. Turnbaugh[4,14 ✉]

Diet is a major factor that shapes the gut microbiome[1], but the consequences of diet-induced changes in the microbiome for host pathophysiology remain poorly understood. We conducted a randomized human intervention study using a very-low-calorie diet (NCT01105143). Although metabolic health was improved, severe calorie restriction led to a decrease in bacterial abundance and restructuring of the gut microbiome. Transplantation of post-diet microbiota to mice decreased their body weight and adiposity relative to mice that received pre-diet microbiota. Weight loss was associated with impaired nutrient absorption and enrichment in *Clostridioides difficile*, which was consistent with a decrease in bile acids and was sufficient to replicate metabolic phenotypes in mice in a toxin-dependent manner. These results emphasize the importance of diet–microbiome interactions in modulating host energy balance and the need to understand the role of diet in the interplay between pathogenic and beneficial symbionts.

Very-low-calorie diets (VLCDs) involve extreme calorie restriction (approximately 800 kcal per day, typically in liquid form[2]). Gut microbiome composition is altered during weight loss induced by VLCDs[3,4]; however, the consequences of this alteration for health and disease remain unclear. To address this knowledge gap, we performed an exploratory analysis in a trial of 80 post-menopausal women who were overweight or obese and were randomized to either a medically supervised weight loss program or to a control group instructed to maintain a stable weight for 16 weeks (Extended Data Fig. 1a). The primary outcomes—changes in muscle mass and myocellular insulin sensitivity—are reported elsewhere[5]. The weight loss program included 8 weeks of VLCD (800 kcal per day), 4 weeks of a conventional low-calorie diet (CONVD), and 4 weeks of weight maintenance (MAINT; Extended Data Fig. 1b). Both groups had similar baseline characteristics (Supplementary Table 1). The intervention group showed a weight reduction of 13.6 ± 4.0% (mean ± s.d.) relative to baseline, which corresponds to a loss of 12.5 ± 3.9 kg after 12 weeks (Fig. 1a). Total caloric and macronutrient intake was lower during the VLCD, CONVD, and MAINT phases than at baseline (Extended Data Fig. 1c, d). The VLCD lowered proportional fat intake from baseline, whereas relative macronutrient intake was comparable to baseline in the CONVD and MAINT phases (Extended Data Fig. 1e, Supplementary Table 2). The VLCD led to decreased adiposity (Extended Data Fig. 1f) and improved glucose regulation (Extended

Data Fig. 1g). Glucose regulation reverted after CONVD despite the maintenance of lower adiposity; both phenotypes were unchanged in the control group.

Diet restructures the gut microbiome

Consistent with the hypothesis that sustained caloric restriction during the VLCD could have pronounced impacts on the gut microbiota—analogous to the effects of long-term fasting[6,7] or parenteral nutrition[8]—the VLCD significantly decreased the level of gut microbial colonization measured both by faecal DNA content (Extended Data Fig. 2a) and 16S rRNA gene copies (Fig. 1b). Next, we performed 16S ribosomal RNA (rRNA) gene sequencing on 207 samples from 70 individuals (Supplementary Table 3). The number of denoised 16S rRNA amplicon sequence variants (ASVs) was increased after the VLCD but returned to baseline levels during the CONVD (Fig. 1c). The VLCD also induced a marked, but reversible, shift in gut microbial community structure. Quantification of community distances from baseline for each individual identified a significant perturbation following the VLCD that reverted during subsequent diet phases (Extended Data Fig. 2b, c). Multivariate comparison also showed that the VLCD induced significant differences from the baseline microbiota ($P < 0.01$; ADONIS with Bray–Curtis dissimilarity). Reproducible shifts were apparent via principal coordinates analysis

[1]Charité Universitätsmedizin Berlin, Department of Endocrinology and Metabolic Diseases, Berlin, Germany. [2]Berlin Institute of Health (BIH), Berlin, Germany. [3]DZHK (German Centre for Cardiovascular Research), partner site Berlin, Center for Cardiovascular Research (CCR), Berlin, Germany. [4]Department of Microbiology & Immunology, University of California San Francisco, San Francisco, CA, USA. [5]Gladstone Institutes, San Francisco, CA, USA. [6]Center for Molecular Toxicology and Carcinogenesis, Department of Veterinary and Biomedical Sciences, The Pennsylvania State University, University Park, PA, USA. [7]Department of Pathology, University of California San Francisco, San Francisco, CA, USA. [8]Department of Laboratory Medicine, University of California San Francisco, San Francisco, CA, USA. [9]Department of Epidemiology & Biostatistics, University of California San Francisco, San Francisco, CA, USA. [10]Institute for Human Genetics, University of California San Francisco, San Francisco, CA, USA. [11]Institute for Computational Health Sciences, University of California San Francisco, San Francisco, CA, USA. [12]Chan Zuckerberg Biohub, San Francisco, CA, USA. [13]These authors contributed equally: Reiner Jumpertz von Schwartzenberg, Jordan E. Bisanz. [14]These authors jointly supervised this work: Joachim Spranger, Peter J. Turnbaugh. ✉e-mail: joachim.spranger@charite.de; peter.turnbaugh@ucsf.edu
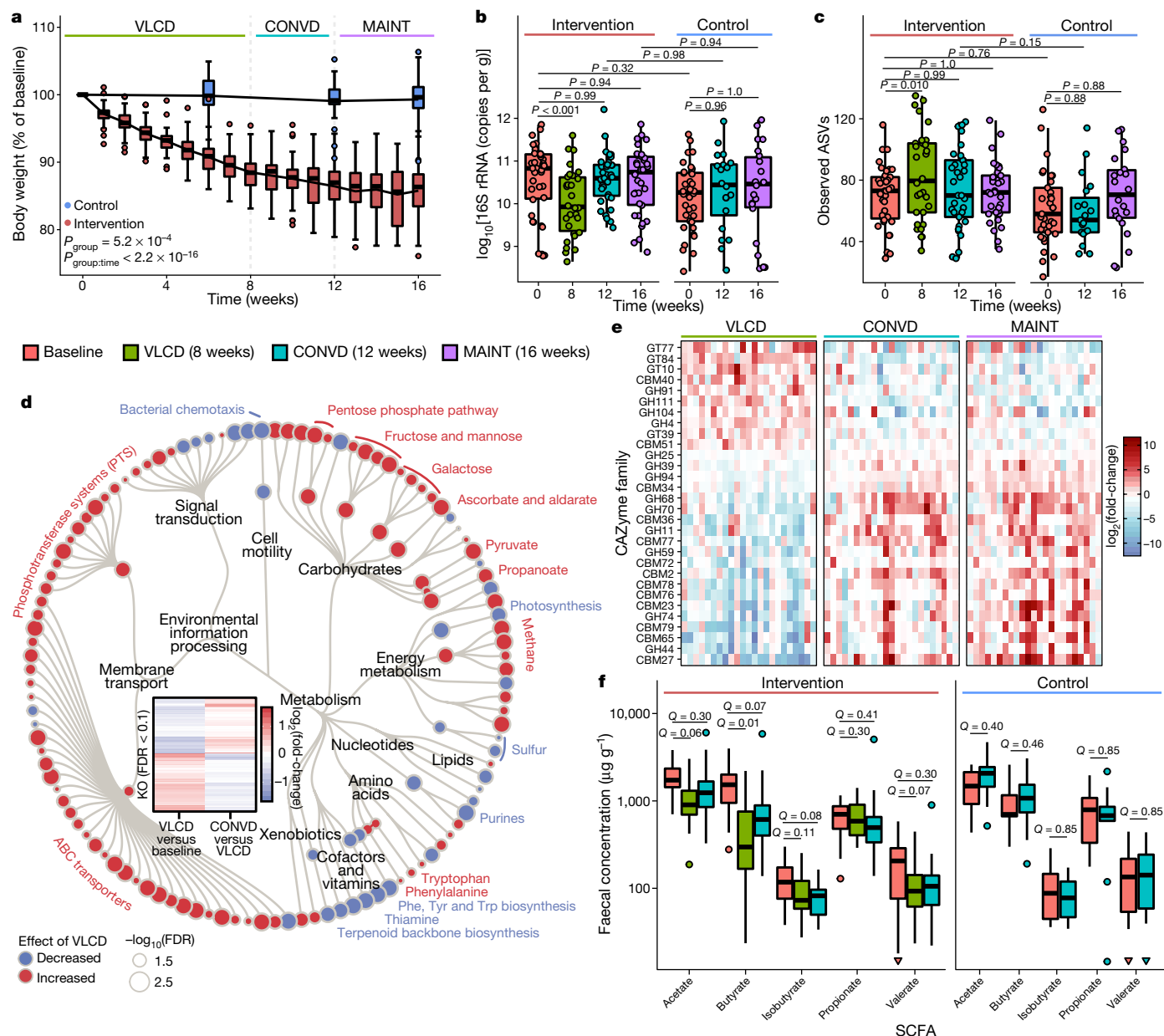
**Fig. 1 | Very low-calorie diets alter microbiota composition and activity.**
a, Diet participants lost significantly more weight over time than controls over the combined 12-week intervention (0.84% per week (0.68–1.0 95% confidence interval (CI)), $P < 2.2 \times 10^{-16}$, LMM; $n_{control} = 40$, $n_{intervention} = 40$ participants). **b**, The VLCD decreased overall gut microbial colonization (qPCR-based quantification of 16S rRNA gene copies per gram wet weight; $P < 0.001$, LMM; $n_{intervention} = 39$, $n_{control} = 35$ participants). **c**, Richness of 16S rRNA ASVs increased following the consumption of VLCD ($P = 0.010$, negative binomial generalized LMM; $n_{intervention} = 37$, $n_{control} = 32$ participants). **d**, Microbiome functional capacity (measured by shotgun metagenomic sequencing) is altered by VLCD (Supplementary Table 4; FDR $Q < 0.1$, Limma and mROAST). The tree demonstrates a functional hierarchy; inner nodes and outer tips represent pathways and modules, respectively. Inset, a heatmap of KOs that differed

significantly between VLCD and baseline shows that they reverted in the CONVD phase (Extended Data Fig. 2i). **e**, Heat map of diet-induced changes to CAZymes compared to baseline (FDR $Q < 0.1$, two-sided paired t-test VLCD versus baseline) demonstrates that changes revert during CONVD and MAINT phases (Supplementary Table 5). **f**, The SCFAs acetate, butyrate, and valerate are significantly reduced in stool samples during during VLCD ($n_{intervention} = 18$, $n_{control} = 10$ participants per time point; FDR $Q < 0.1$, two-sided Wilcoxon signed-rank test; downward triangles represent a concentration below $10 \, \mu g \, g^{-1}$). Statistical analysis carried out using linear mixed effects models (LMM) with participant as random effect and Tukey all-pair two-sided comparison unless otherwise noted. In boxplots: centre line, median; box, first and third quartiles; whiskers, 1.5× interquartile range (IQR) with outliers individually plotted.

(Extended Data Fig. 2d). To identify bacterial markers of VLCD, we fit a random forest classifier of baseline versus VLCD in the intervention group as a function of genus-summarized abundances (Extended Data Fig. 2e). Tenfold cross-validation showed that the best classifier was based on 30 bacterial genera with minimal error (11.94%). These genera reverted to baseline levels during the CONVD phase. Closer inspection

of the predictive genera showed that the VLCD increased the growth of bacteria capable of foraging on host glycans (*Akkermansia*) at the expense of bacteria specialized for the metabolism of plant polysaccharides (*Roseburia*, *Ruminococcus*, *Eubacterium*)[9,10].

To more directly assess gut bacterial metabolic capacity, we performed metagenomic sequencing on 29 participants in the intervention
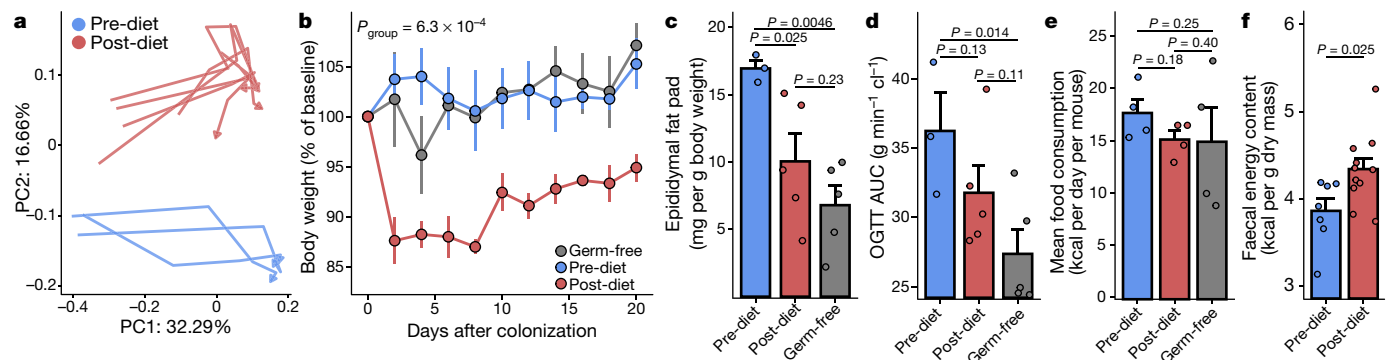
Fig. 2 | Weight loss and improved metabolic health are transmissible via the gut microbiome. a, Principal coordinates analysis of unweighted UniFrac distances showing that compositionally distinct communities were established in mice that received transplantation of stool samples from individuals at baseline (pre-diet, $n = 3$) or after the combined intervention (post-diet, $n = 5$) across all time points with early temporal instability ($P_{time} = 0.0001$, $R^2 = 0.17$; $P_{group} = 0.0001$, $R^2 = 0.18$, ADONIS). Each mouse is represented as a vector over time terminating with an arrow (day 21). **b**, Post-diet recipient mice lost significant weight compared with GF and pre-diet recipient mice (12.2% (6.5–17.8 95% CI), $P = 0.0014$, LMM). **c**, Pre-diet recipient mice showed increased adiposity compared to post-diet recipient

mice ($P = 0.025$) and GF controls ($P = 0.0046$). **d**, Colonization with pre-diet stool samples increased glucose tolerance on an oral glucose tolerance test (OGTT) as compared to GF controls ($P = 0.014$). AUC, area under the curve. For **b**–**d**, $n_{pre-diet} = 3$, $n_{post-diet} = 5$, $n_{GF} = 5$ mice) **e**, Food consumption did not differ between groups ($P = 0.63$, $n = 4$ time intervals normalized to n_{mice} and interval length in days). **f**, Stool energy density (kcal per g dry mass) was increased in mice colonized with the post-diet microbiome ($P = 0.025$, LMM, collected at days 1 ($n_{pre-diet} = 2$, $n_{post-diet} = 3$ mice), 3 ($n_{pre-diet} = 2$, $n_{post-diet} = 4$ mice), and 7 ($n_{pre-diet} = 3$, $n_{post-diet} = 4$ mice)). Data presented as mean ± s.e.m. where applicable and statistical analysis carried out using a Kruskal–Wallis test with Dunn's two-sided post hoc test unless otherwise noted.

group and 18 control subjects (selected on the basis of completeness of longitudinal sampling; Supplementary Table 3). Consistent with our amplicon data, metagenomic analysis showed that gut microbial community structure was transiently perturbed after the VLCD phase (Extended Data Fig. 2f–h). Metabolic reconstructions identified 88 pathways, 100 modules, and 1,502 Kyoto Encyclopedia of Genes and Genomes (KEGG) orthologies (KOs) whose abundances differed between the VLCD and baseline samples (false discovery rate (FDR) $Q < 0.1$, Supplementary Table 4). Comparison of baseline and CONVD samples showed more modest differences, with only eight differentially abundant KOs (Extended Data Fig. 2i). Next, we plotted VLCD-differential KEGG features in a functional hierarchy[11] (Fig. 1d). After the VLCD there were broad increases in the relative abundance of membrane transporters and enzymes involved in the import and metabolism of saccharides or the production of short chain fatty acids (SCFAs; Supplementary Table 4). The observed shifts in microbial community metabolic potential were reversible; KOs that changed in abundance during VLCD reverted during CONVD (Fig. 1d, inset).

The VLCD had a pronounced effect on the abundance of bacterial genes involved in dietary and host glycan metabolism. We mapped reads to carbohydrate-active enzymes (CAZymes)[12], and found that 30 were significantly altered by the VLCD (FDR $Q < 0.1$; Fig. 1e, Supplementary Table 5). The VLCD led to a reduction in the abundance of CAZymes involved in processing plant-derived carbohydrates and an increase in capacity to metabolize ingredients in the VLCD formulation (inulin lyase (CAZyme ID GH91)), mucosal glycans (sialic acid (CBM40)), and glycosaminoglycans (keratan sulfate (GH111)). CAZymes were mostly restored to baseline levels following CONVD; six families of CAZymes still showed differences in abundance compared to the baseline (Supplementary Table 5). These results suggest that the VLCD induced marked changes in both the structure and metabolic activity of the human gut microbiome and promoted the expansion of bacteria that can feed on host glycans.

To further assess the effects of VLCD on microbial metabolism, we quantified two major end-products (SCFAs and branched chain amino acids (BCAAs)) using targeted mass spectrometry in a subset of participants that were selected on the basis of sample availability ($n = 18$ intervention, $n = 10$ control). The VLCD significantly decreased the concentration of the BCAA leucine, with a trend towards decreased

isoleucine and valine (Extended Data Fig. 2j). All three BCAAs were significantly decreased at the CONVD time point. Three major SCFAs produced by the gut microbiome (acetate, butyrate, and valerate) were all significantly decreased during the VLCD phase (Fig. 1f). Thus, although the relative abundance of genes involved in SCFA biosynthesis increased on the VLCD, this was insufficient to compensate for the overall decrease in microbial colonization (Extended Data Fig. 2k, l).

Weight loss is transmissible to mice

Transplantation of the human gut microbiota into germ-free mice (humanization) indicated that dietary perturbations to the gut microbiome contribute to weight loss. We selected the five participants that lost the most weight following the 3-month intervention; these individuals lost 55.6% more body weight than the average of the remaining cohort (Extended Data Fig. 3a). We transplanted stool samples collected from these five donors before (pre-diet) and after the 12 weeks of combined dietary intervention (post-diet) into germ-free (GF) adult male C57BL/6J mice, after which the two recipient groups were maintained in separate isolators until the experimental endpoint (Extended Data Fig. 3b). We used 16S rRNA gene sequencing and confirmed that there were stable differences in microbiota between the two recipient groups (Fig. 2a) that recapitulated the differences between the microbiota of humans before and after the diet period, including 58 ASVs (Extended Data Fig. 3c, Supplementary Table 6). Inferred gene abundance[13] identified 392 KOs that differed significantly between the colonization groups (more than twofold difference; FDR $Q < 0.1$, linear mixed effects model (LMM); Supplementary Table 7), which showed that functional capacity in central pathways of carbon, fatty acid, and amino acid metabolism had been altered by caloric restriction (Extended Data Fig. 3d).

Microbiome transplantation was sufficient to induce multiple phenotypes found in human subjects during weight loss. Within 2 days of colonization, post-diet sample recipients had lost 12.4 ± 5.2% of their body mass (mean ± s.d.); this was significantly more than the pre-diet recipients or GF controls, and the weight loss was maintained for 21 days after colonization (Fig. 2b). Body fat was also significantly affected by the post-diet gut microbiome (Fig. 2c), as these mice did not show the increase in adiposity that is typically found after colonization[14]. Pre-diet
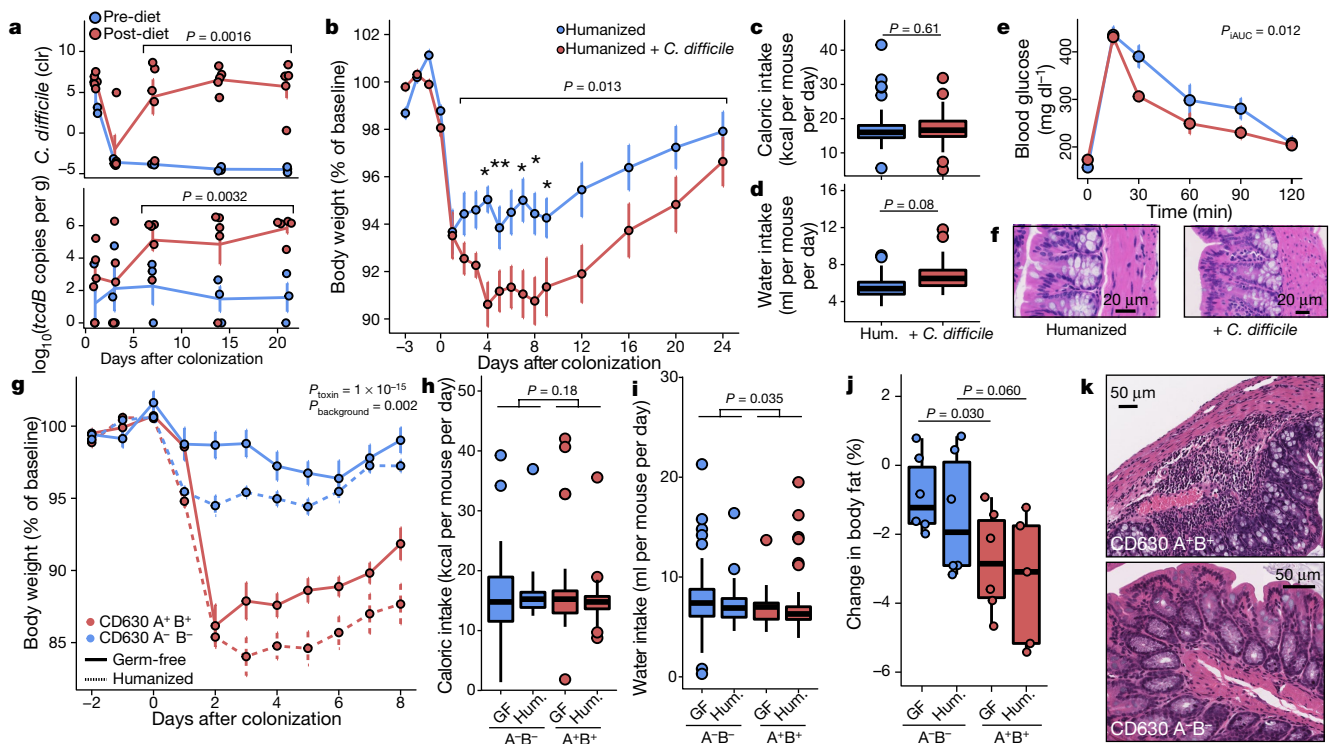
Fig. 3 | Endogenous *C. difficile* is unrestricted by the post-diet microbiota and contributes to weight loss in a toxin-dependent manner. a, Sequencing (top; centred $\log_2$(ratio), clr) and qPCR (bottom) show that *C. difficile* and *tcdB* are significantly higher in post-diet recipient mice than in pre-diet recipient mice ($P = 0.0016$ and $P = 0.0032$, respectively, LMM; $n_{\text{pre-diet}} = 3$, $n_{\text{post-diet}} = 5$ mice). **b**, Addition of *C. difficile* JBZPo1 spores to a reference donor sample is sufficient to replicate the increase in weight loss in recipient mice compared with human microbiota with vehicle control ($P = 0.013$, estimate derived from the model = 3.4% (1.2–5.7 95% CI), LMM 2–24 days after colonization, *$P < 0.05$ two-sided Welch's *t*-test at individual time points; $n = 6$ mice per group). **c**, **d**, Daily food consumption (**c**; $P = 0.61$, LMM, $n = 6$ mice per group measured over 13 intervals), and water consumption (**d**; $P = 0.08$, LMM, $n = 6$ mice per group measured over 14 intervals) were not significantly different in recipient mice with or without *C. difficile*. **e**, Oral glucose tolerance test shows improved response in mice colonized with *C. difficile* ($P = 0.012$, two-sided Welch's *t*-test

of incremental AUC, $n = 6$ mice per group). **f**, Colon tissue does not show gross evidence of colitis (representative images, $n = 6$ mice per group; scoring in Extended Data Fig. 6f). **g**, *C. difficile* induced weight loss in both GF and humanized mice in a toxin-dependent manner (LMM). **h**, Food consumption was not different between mice that received different genotypes of *C. difficile* ($P = 0.18$, LMM). **i**, Mice that received toxin-deficient *C. difficile* consumed more water than those that received toxigenic *C. difficile* ($P = 0.035$, difference 2.3 ml (0.3–4.3 95% CI), LMM). **j**, Colonization with toxigenic *C. difficile* reduced body fat ($P = 0.03$ GF, $P = 0.06$ humanized, Kruskal–Wallis test with Dunn's two-sided post hoc test; $n = 5$–6 per group as in Extended Data Fig. 8a for **g**–**j**). **k**, Representative histology demonstrates neutrophil infiltration in the toxigenic strain (Extended Data Fig. 8e). Statistical analysis carried out using LMM and Tukey two-sided all-pair comparison unless otherwise noted. Data shown as mean ± s.e.m. In boxplots: centre line, median; box, first and third quartiles; whiskers, 1.5× IQR with outliers individually plotted.

colonization significantly impaired glucose tolerance compared to GF mice (Fig. 2d), whereas the post-diet group showed a smaller difference. There were no significant differences in caloric intake across the three groups (Fig. 2e); however, the caloric density of faeces was significantly higher in the post-diet recipients than the pre-diet recipients (Fig. 2f). Replication experiments with newly prepared pools of stool samples taken at the 12-week (Extended Data Fig. 4a–c) and 8-week diet points from these five individuals (Extended Data Fig. 4d–g), and samples taken at the 12-week point from the four individuals who were closest to the median weight loss (Extended Data Fig. 4h–j), reproduced features of the initial experiment, indicating that the phenotypic consequences of diet-induced shifts in the gut microbiome are robust and not necessarily restricted to severe weight loss. Thus, the post-diet human gut microbiome contributes to weight loss in part by decreasing the efficiency of dietary energy absorption; however, microbiome-induced changes to host energy expenditure and/or resting metabolic rate remain to be explored[15].

Endogenous *C. difficile* is implicated

Closer inspection of the humanization experiments showed that the microbiota of mice that received post-diet faecal samples were enriched

with the enteric pathogen *C. difficile* (Fig. 3a, Extended Data Fig. 3c). The gene family that showed the greatest difference in abundance (Supplementary Table 7) between the two recipient groups represents *C. difficile* A/B toxins (KO K11063, FDR $Q < 0.05$, LMM), which we confirmed independently through quantitative PCR (qPCR) of the *tcdB* gene (Fig. 3a). *C. difficile* and *tcdB* were detectable at similar abundances in both recipient groups at baseline, but were maintained at abundances orders of magnitude lower in pre-diet recipients, which shows that the difference between the two groups resulted from an altered ability to restrict growth of *C. difficile* rather than a difference in initial exposure (Fig. 3a). Endpoint samples from mice in both groups tested positive for the toxins TcdA and TcdB and for *C. difficile* by PCR and culture, respectively; however, only animals in the post-diet group had detectable levels of toxin as measured by enzyme-linked immunosorbent assay (ELISA; Extended Data Fig. 3e). Toxin was not consistently detected in our subsequent experiments (Extended Data Fig. 4k, l), which might have contributed to variation in host metabolic phenotypes.

Given the high degree of between-strain variability observed in *C. difficile*–host interactions[16], we isolated and sequenced *C. difficile* JBZPo1 from the caecum of a post-diet recipient mouse (Extended Data Fig. 5a) and used metagenomic sequencing to confirm that the correct strain

Article

was isolated (see Methods). Additional typing of this strain revealed that it encoded toxins TcdA and TcdB, but not the binary toxin associated with hypervirulent *C. difficile*[16] (Extended Data Fig. 5b, c). Multilocus sequence typing and phylogenetic analysis (Extended Data Fig. 5d) indicated that JBZPo1 belongs to the ST2 clade (likely ribotype 014-20) of non-hypervirulent *C. difficile*, which is among the most commonly isolated groups in Europe[17].

To test whether *C. difficile* is sufficient to replicate weight loss and metabolic phenotypes, we colonized individually housed GF C57BL/6J mice with a post-VLCD human specimen, or the same sample with the addition of *C. difficile* JBZPo1 spores (Extended Data Fig. 6a). The human post-VLCD donor sample was sufficient to induce weight loss (maximum loss $6.3 \pm 2.3\%$ (mean $\pm$ s.d.) at day 1); however, the addition of the *C. difficile* spores led to increased and sustained weight loss over the duration of the experiment (maximal loss $9.4 \pm 2.3\%$ at day 4; Fig. 3b) without causing dehydration (Extended Data Fig. 6b). Food and water consumption were not significantly different (Fig. 3c, d). In addition, *C. difficile* significantly improved glucose tolerance (Fig. 3e). Although we detected no differences in adiposity at baseline, the *C. difficile*-colonized mice had significantly increased final adiposity relative to controls (Extended Data Fig. 6c). Despite the clear measurable presence of *C. difficile* and its toxins in these mice (Extended Data Fig. 6d, e) and absence in the humanized controls, there were no signs of abnormal posture, behaviour, or stool consistency. Gross examination of proximal colon histology did not reveal typical markers of *C. difficile*-associated colitis, such as haemorrhage, oedema, and mucosal separation (Fig. 3f); however, scoring by a pathologist blinded to interventions identified minor neutrophil infiltration with reactive changes associated with *C. difficile* colonization (Extended Data Fig. 6f).

Diet decreases colonization resistance

Next, we sought to test whether diet-induced shifts in the gut microbiome influence colonization resistance to *C. difficile* and thus host physiology. We colonized mice with faecal samples taken from the reference donor at each of the diet phases and inoculated with JBZPo1 spores (Extended Data Fig. 7a). In both VLCD and CONVD phases, significantly enhanced weight loss was observed relative to the baseline colonization group (4.6% and 6.6% respectively, Extended Data Fig. 7b). *C. difficile* colonization was similar across groups and time; however, significantly more TcdB was detected 2 days after colonization in mice that had received transplantation of CONVD samples, suggesting that diet–microbiota interactions may affect both the outgrowth and expression of *C. difficile* virulence traits (Extended Data Fig. 7c, d).

To establish whether the effects of *C. difficile* on weight and metabolism are mediated by the virulence factors TcdA and TcdB, we obtained a toxin-deficient mutant of *C. difficile* 630[18] and used it to replicate the experiment in GF and humanized mice (Extended Data Fig. 8a). Weight loss was induced in a toxin-dependent manner irrespective of colonization background (Fig. 3g), despite comparable food intake (Fig. 3h). Colonization with the TcdA/B⁺ strain led to a minor but significant decrease in water intake compared to the TcdA/B⁻ strain (Fig. 3i), without any detectable signs of dehydration (Extended Data Fig. 8b), and significantly decreased body fat (Fig. 3j). *C. difficile* was more abundant in mono-colonized mice, but toxin levels were comparable to those in humanized mice (Extended Data Fig. 8c, d). In mice colonized with the toxigenic *C. difficile* 630 strain, which was originally isolated from severe pseudomembranous colitis[19], we observed more severe histological markers of colitis (Fig. 3k, Extended Data Fig. 8e), emphasizing the utility of isolating relevant strains from the cohorts analysed in this study.

We next sought to determine the relevance of these observations to our diet cohort and the original top five weight losers. Although all participants were otherwise asymptomatic, screening of the five participants that lost the most weight revealed that all donors appeared to have carried *C. difficile* at some point during the intervention (on
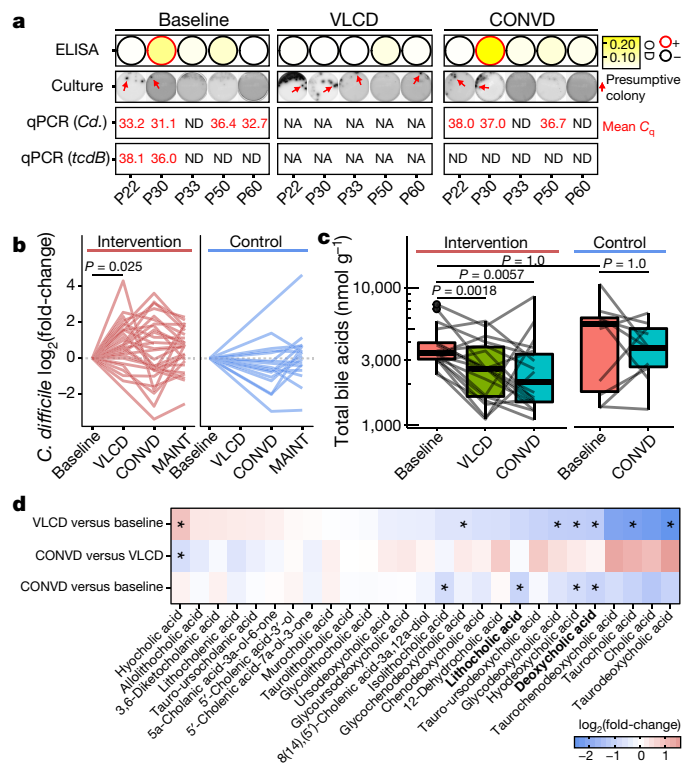
Fig. 4 | Caloric restriction is associated with an expansion of *C. difficile* and altered bile acid pools. a, *C. difficile* presence in the five individuals with the highest weight loss, measured by faecal ELISA for *C. difficile* toxins (TcdA/B), selective and differential culture, and qPCR targeting the *C. difficile* 16S rRNA gene (*Cd.*) and the toxin B gene (*tcdB*). Yellow shading shows normalized optical density (OD) for the ELISA with OD > 0.123 taken as a positive reaction. Culture plates imaged under long-wave UV show the presence of presumptive *C. difficile* colonies (red arrows: fluorescent colonies with ground-glass appearance and filamentous edges, representative plate shown under white light in Extended Data Fig. 9e). qPCR results are represented as the cycle of quantification (C_q) at which FAM-fluorescence was detected. NA, not assayed; ND, not detected. **b**, *C. difficile* abundance in humans, determined from metagenomic sequencing, was significantly increased during VLCD with no other significant contrasts (log₂ fold difference = 0.88 ± 0.28 (mean $\pm$ s.e.), $P = 0.025$, LMM with Tukey's two-sided all-pair comparison; $n_{intervention} = 29$, $n_{control} = 18$ participants). **c**, Dietary intervention significantly decreased total bile acid pools in human participants ($n_{intervention} = 20$, $n_{control} = 10$ participants; LMM with Tukey's two-sided all-pair comparison). Centre line, median; box, first and third quartiles; whiskers, 1.5× IQR with outliers individually plotted. **d**, Differential bile acid analytes in response to diet ($n = 20$, FDR-corrected two-sided Wilcoxon signed-rank test, *FDR $Q < 0.1$).

the basis of toxin ELISA, culture, and/or qPCR; Fig. 4a). To understand how this may be representative of the complete cohort, we turned to our metagenomic data, which revealed the presence of *C. difficile* at low abundances with a median ranked species abundance of 297 (range, 52–613). *C. difficile* abundance varied among diet intervention participants but increased during the VLCD phase in the intervention group (Fig. 4b).

Given the previously established role of bile acids in modulating growth and germination of *C. difficile*[20,21], we quantified bile acid concentrations in donors for whom we had complete longitudinal faecal collections for the first three diet phases (Supplementary Table 8). Total bile acid pools were significantly decreased in response to VLCD and CONVD (Fig. 4c). We also detected significant decreases in *C. difficile*-inhibitory deoxycholic acid and lithocholic acid[21] in response to diet (Fig. 4d), consistent with our colonization resistance experiment

(Extended Data Fig. 7e). The decrease in bile acids probably reflects a combination of reduced gallbladder emptying of primary bile acids (due to decreased fat consumption[22]; Extended Data Fig. 1c), an overall decrease in bacterial colonization (Fig. 1b), and shifts in the abundance of bile acid-metabolizing taxa (Extended Data Fig. 2e, h). The metabolite changes observed across the overall cohort were also reflected in the five donors used for our original microbiome transplantation experiment (Extended Data Fig. 9a–c).

Limitations and implications

There are multiple limitations of this work. Our clinical trial was performed at a single research site, resulting in limited sampling of geographical and ethnic backgrounds. We analysed a single VLCD preparation; more work is needed to assess the generalizability of these findings to alternative formulations, including the potential impact of food matrix and preparation method[23]. *C. difficile* colonization across the full cohort was based on metagenomics. Attempts to detect toxin-positive *C. difficile* carriage using a commercial testing platform (Cepheid Xpert) failed, potentially because of the assay design and the weak diagnostic value of detecting asymptomatic carriage[24] and/or the prolonged storage of these samples at the time of testing. Estimates of asymptomatic carriage of *C. difficile* range widely from 0–90% of individuals surveyed[25] as a function of age, exposure to health care settings, and methodology, with a recent meta-analysis demonstrating a rate of 8.1% on inpatient admission[26]. Finally, our microbiome results were exploratory outcomes of this intervention study[5]; the clinical relevance of the association between *C. difficile* and weight loss outcomes requires additional human studies that specifically correlate asymptomatic carriage and metabolic outcomes.

Despite these limitations, our work clearly demonstrates that severe calorie restriction leads to significant, but reversible, shifts in the human gut microbiome. Mice colonized with post-diet microbiota replicated human phenotypes, including decreased weight and adiposity, driven in part by an inability to restrict the growth of *C. difficile*. We propose a working model through which diet and *C. difficile* conspire to shape host energy balance (Extended Data Fig. 9d). More broadly, this study emphasizes the utility of coupling well-controlled clinical interventions with humanized mice, enabling the mechanistic dissection of complex relationships between the host, microbiome, and enteric pathogens.

Online content

Any methods, additional references, Nature Research reporting summaries, source data, extended data, supplementary information, acknowledgements, peer review information; details of author contributions and competing interests; and statements of data and code availability are available at https://doi.org/10.1038/s41586-021-03663-4.

1. David, L. A. et al. Diet rapidly and reproducibly alters the human gut microbiome. *Nature* **505**, 559–563 (2014).
2. Johansson, K., Neovius, M. & Hemmingsson, E. Effects of anti-obesity drugs, diet, and exercise on weight-loss maintenance after a very-low-calorie diet or low-calorie diet: a systematic review and meta-analysis of randomized controlled trials. *Am. J. Clin. Nutr.* **99**, 14–23 (2014).
3. Louis, S., Tappu, R. M., Damms-Machado, A., Huson, D. H. & Bischoff, S. C. Characterization of the gut microbial community of obese patients following a weight-loss intervention using whole metagenome shotgun sequencing. *PLoS ONE* **11**, e0149564 (2016).
4. Heinsen, F.-A. et al. Beneficial effects of a dietary weight loss intervention on human gut microbiome diversity and metabolism are not sustained during weight maintenance. *Obes. Facts* **9**, 379–391 (2016).
5. Spranger, L. et al. Thrifty energy phenotype predicts weight regain — results of a randomized controlled trial. Preprint at https://www.medrxiv.org/content/10.1101/2021.03.25.21254300v1 (2021).
6. Kohl, K. D., Amaya, J., Passement, C. A., Dearing, M. D. & McCue, M. D. Unique and shared responses of the gut microbiota to prolonged fasting: a comparative study across five classes of vertebrate hosts. *FEMS Microbiol. Ecol.* **90**, 883–894 (2014).
7. Zarrinpar, A., Chaix, A., Yooseph, S. & Panda, S. Diet and feeding pattern affect the diurnal dynamics of the gut microbiome. *Cell Metab.* **20**, 1006–1017 (2014).
8. Harris, J. K. et al. Specific microbiome changes in a mouse model of parenteral nutrition associated liver injury and intestinal inflammation. *PLoS ONE* **9**, e110396 (2014).
9. van Passel, M. W. et al. The genome of *Akkermansia muciniphila*, a dedicated intestinal mucin degrader, and its use in exploring intestinal metagenomes. *PLoS ONE* **6**, e16876 (2011).
10. Morrison, D. J. & Preston, T. Formation of short chain fatty acids by the gut microbiota and their impact on human metabolism. *Gut Microbes* **7**, 189–200 (2016).
11. Uchiyama, T., Irie, M., Mori, H., Kurokawa, K. & Yamada, T. FuncTree: functional analysis and visualization for large-scale omics data. *PLoS ONE* **10**, e0126967 (2015).
12. Lombard, V., Golaconda Ramulu, H., Drula, E., Coutinho, P. M. & Henrissat, B. The carbohydrate-active enzymes database (CAZy) in 2013. *Nucleic Acids Res.* **42**, D490–D495 (2014).
13. Langille, M. G. et al. Predictive functional profiling of microbial communities using 16S rRNA marker gene sequences. *Nat. Biotechnol.* **31**, 814–821 (2013).
14. Bäckhed, F. et al. The gut microbiota as an environmental factor that regulates fat storage. *Proc. Natl Acad. Sci. USA* **101**, 15718–15723 (2004).
15. Cani, P. D. et al. Microbial regulation of organismal energy homeostasis. *Nat. Metab.* **1**, 34–46 (2019).
16. Hunt, J. J. & Ballard, J. D. Variations in virulence and molecular biology among emerging strains of *Clostridium difficile*. *Microbiol. Mol. Biol. Rev.* **77**, 567–581 (2013).
17. Bauer, M. P. et al. *Clostridium difficile* infection in Europe: a hospital-based survey. *Lancet* **377**, 63–73 (2011).
18. Kuehne, S. A. et al. The role of toxin A and toxin B in *Clostridium difficile* infection. *Nature* **467**, 711–713 (2010).
19. Wüst, J., Sullivan, N. M., Hardegger, U. & Wilkins, T. D. Investigation of an outbreak of antibiotic-associated colitis by various typing methods. *J. Clin. Microbiol.* **16**, 1096–1101 (1982).
20. Buffie, C. G. et al. Precision microbiome reconstitution restores bile acid mediated resistance to *Clostridium difficile*. *Nature* **517**, 205–208 (2015).
21. Sorg, J. A. & Sonenshein, A. L. Bile salts and glycine as cogerminants for *Clostridium difficile* spores. *J. Bacteriol.* **190**, 2505–2512 (2008).
22. Festi, D. et al. Gallbladder motility and gallstone formation in obese patients following very low calorie diets. Use it (fat) to lose it (well). *Int. J. Obes. Relat. Metab. Disord.* **22**, 592–600 (1998).
23. Carmody, R. N. et al. Cooking shapes the structure and function of the gut microbiome. *Nat. Microbiol.* **4**, 2052–2063 (2019).
24. Fang, F. C., Polage, C. R. & Wilcox, M. H. Point-counterpoint: what is the optimal approach for detection of *Clostridium difficile* infection? *J. Clin. Microbiol.* **55**, 670–680 (2017).
25. Furuya-Kanamori, L. et al. Asymptomatic *Clostridium difficile* colonization: epidemiology and clinical implications. *BMC Infect. Dis.* **15**, 516 (2015).
26. Zacharioudakis, I. M., Zervou, F. N., Pliakos, E. E., Ziakas, P. D. & Mylonakis, E. Colonization with toxinogenic *C. difficile* upon hospital admission, and risk of infection: a systematic review and meta-analysis. *Am. J. Gastroenterol.* **110**, 381–390, quiz 391 (2015).

Article

Methods

MMS (Muscle Metabolism Study) human cohort

Recruitment. Between March 2012 and July 2015, we randomized 80 post-menopausal women who were overweight or obese to either undergo a medically supervised weight loss and lifestyle intervention program (details below) or to remain weight stable over a period of 16 weeks. This outpatient study was conducted in our experimental and clinical research centre (ECRC, Charité Campus Berlin-Buch) and participants were recruited via newspaper ads or via the endocrinological outpatient clinic. The last volunteers finished the study in September 2017, when the study ended owing to completion. We used a stratified randomization scheme based on three BMI (body mass index: weight (kg)/height (m))^2 strata at baseline. Recruiting study nurses and physicians were blinded to the allocation sequence until inclusion of the volunteer. The allocation sequence was made via a random computer-generated list by the study PI (K.M.). Participants were recruited and allocated to the interventions by study physicians. The study was registered at www.clinicaltrials.gov under NCT01105143. The study was approved by the Ethik-Kommission der Charité-Universitätsmedizin Berlin. The study protocol is included as Supplementary Data File 1 and the Consort 2010 Checklist is provided in Supplementary Table 9. Informed consent was obtained from each study volunteer before study participation. The following conditions were used as exclusion criteria: weight loss of more than 5 kg in the last 2 months, severe chronic diseases including cancer within the last 5 years, severe heart disease, severe impairment of hepatic or renal function, severe anaemia or disturbed coagulation, eating disorders or any other psychiatric condition that would interact with the trial intervention, malabsorption, acute or chronic infections, severe hypertension, myopathy, food allergies, any other uncontrolled endocrine disorder, and changes in smoking habits, diets or medication that strongly affect energy homeostasis within the last 3 months before the study. The post-menopause status was ensured by medical history (cessation of the monthly period) and follicle stimulating hormone (FSH) screens if the status was unclear. The primary outcomes of the study were to examine the effects of negative energy balance on regulation of skeletal muscle mass and myocellular insulin sensitivity. As secondary outcomes, a variety of systems-based approaches were used to comprehensively characterize physiological responses to negative energy balance, including analysis of microbial taxonomic and gene abundances, given previous reports that microbiome composition correlates with nutrient absorption and body composition[14] (Supplementary Data File 1). As such, the study was not designed to be powered for these specific microbiome analyses. The study protocol was amended to include the microbiome analysis and approved before recruitment. No additional documentation or consent was required for inclusion of participants in the microbiome component of the study.

Intervention. After baseline phenotyping, volunteers belonging to the intervention group were placed on an 800 kcal/d liquid diet (Optifast, Nestlé) accompanied by weekly group meetings and weight loss counselling for 2 months. Thereafter, the diet was switched to a low calorie (individual daily caloric goals derived from baseline resting metabolic rate over 24 h) diet with 50–55% of total kcals derived from carbohydrates, 15–20% from protein and ~30% from fat according to a food pyramid (as recommended by the German Nutrition Society, DGE) and volunteers in the intervention group only were additionally instructed to take at least 10,000 steps per day. After 4 weeks (month 3), the weight loss intervention was completed and phenotyping was repeated. Subsequently, volunteers were instructed to maintain their weight by changing daily caloric intake goals to calories from the initial metabolic rate plus 500 kcal. Adjustments of individual intake goals were made according to body weight to achieve weight stabilization for another 4 weeks. After this weight stabilization phase, initial phenotyping was repeated.

Volunteers in the control group were instructed to keep their weight stable during the whole first 4 months; this was ensured using monthly visits and nutritional counselling geared towards weight stabilization (resting metabolic rate plus 500 kcal). One volunteer (P15) was included in the study but decided to leave shortly before randomization, which is why no baseline anthropometrics are reported. However, as this volunteer provided baseline stool samples, we chose to include this sample in the microbiome sequencing analysis as a baseline control sample.

Stool samples were collected during each phenotyping visit and additionally after 8 weeks on the liquid diet in the intervention group (Extended Data Fig. 1b). For this, volunteers were given a stool collection kit and instructed to store collected stool samples in the freezer at −20 °C until they were transported in a cooled container to our research unit. All samples were subsequently stored at −80 °C. Dietary information was assessed by dietary records at every phenotyping time point. Volunteers were instructed to note down every food item that was consumed throughout the four days before the phenotyping, including the exact weight or an equivalent estimation (for example, a teaspoon or a cup). Nutrient content was estimated using Prodi v6.2 Expert. The Souci-Fachmann-Kraut-Database 2005 and the German Federal Nutrition Key (Bundeslebensmittelschlüssel) Version 3.01 were used as nutrient databases. However, even these databases do not provide nutrient data for every kind of food item, which is why in some cases it was necessary to select a similar food instead of the actual food named in the dietary record. Therefore, one investigator performed all analyses to ensure the best possible standardization.

DNA extraction and sequencing. DNA was extracted from 207 human faecal samples from 75 individuals (39 intervention and 36 control) using the QIAamp DNA Fast Stool Mini Kit (Qiagen, USA) according to the manufacturer's protocol. 16S rRNA gene PCR was carried out as before using Golay-barcoded 515F/806R primers[27] according to the methods of the Earth Microbiome Project (https://earthmicrobiome.org/). Amplicons were quantified using PicoGreen (Quant-It dsDNA; Life Technologies) and pooled at equimolar concentrations for sequencing on an Illumina MiSeq (250 × 150, V3 reagents) with 10% PhiX after size selection and gel purification (QIAquick Gel Extraction Kit Qiagen). Metagenomic sequencing was performed in 161 stool samples derived from a subgroup of the study cohort (29 intervention, 18 controls; $n = 2$–4 samples per individual). Individuals were selected for the most complete set of phenotypic data, without taking into account inter-group differences in host or microbial phenotypes. DNA extraction, library preparation and sequencing were carried out by Eurofins Genomics, Germany using the NEBNext Ultra DNA Library Prep Kit for Illumina according to the manufacturer's instructions. Metagenomic sequencing was performed on the Illumina HiSeq 2500 platform (2 × 125) with 4 samples per lane.

16S rRNA gene sequencing analysis. Reads were demultiplexed using QIIME v1.9.1 (split_libraries_fastq.py) before denoising and processing with DADA2 v1.1.5[28] under MRO v3.2.5. Taxonomy was assigned using the DADA2 implementation of the RDP classifier[29] using the DADA2 formatted training sets for SILVA123 (http://benjjneb.github.io/dada2/assign.html). A phylogenetic tree was constructed using MUSCLE v3.8.31 and MacQIIME v1.9.1 (make_phylogeny.py) using the FastTree algorithm with midpoint rooting. Samples with fewer than 5,000 reads were filtered out of the datasets. Diversity metrics were generated using Vegan v2.4-3 and Phyloseq v1.20.0 with principal coordinate analysis (PCoA) carried out with Ape v4.1. Principal component analysis (prcomp; PCA) was carried out on centred $\log_2$(ratio) (CLR) normalized genus abundances calculated as $A_{clr} = [\log_2(A_1/g_a), \log_2(A_2/g_a),\dots \log_2(A_n/g_a)]$, where A is a vector of read counts with a prior of 0.5 added and g_a is the geometric mean of all values of A. Cross-sectional analysis of significant features was carried out using ALDEx2 v1.8.0[30,31] using 256

simulations and Benjamini–Hochberg corrected Wilcoxon Q values (paired where appropriate). For plotting purposes, $\log_2$(fold-change) was considered as the difference in median CLR-normalized abundance. Random Forest analysis was carried out using randomForest v4.6.12. A Benjamini–Hochberg FDR of 0.1 was used as the cutoff for statistical significance unless otherwise noted.

Metagenomic analysis. Raw Illumina reads underwent standard quality control with fastq-mcf and host read removal by mapping to the human genome (GRCh38) with Bowtie2[32]. For functional quantification, filtered reads were mapped to the KEGG Orthology database[33] using RAPSearch2[34] and length-normalized read counts were tallied for each KO, with the exclusion of reads that mapped to metazoan versions of KOs. A subsequent adjustment for average genome size was done using MicrobeCensus[35]. Statistical testing was performed with the limma package in R, using voom-normalized expression values with quality weights and the formula -Group × Time wherein the fixed effects were treatment group (diet, control), diet phase (baseline, VLCD, CONVD, maintenance), and their interaction[36]. The differential abundance of KOs was further summarized at the module and pathway levels using mROAST[37]. Counts of CAZyme family abundance were determined by DIAMOND[38] against the CAZy database. FDR corrected paired t-tests of $\log_2$(counts per million) abundances were used to identify modules that were altered by VLCD. To normalize the abundance of butanoyl-CoA:acetoacetate CoA-transferase subunits, their abundance was determined using the reads per kilobase per genome equivalent (RPKG) mapping to the gene family (K01034) derived above and multiplying by the estimated genome equivalents per gram determined from qPCR (using 4.2 16S rRNA copies per genome to convert from 16S rRNA copies to genome equivalents). Microbial taxonomy abundances derived from shotgun sequencing were determined using Kaiju[39]. Quantification of *C. difficile* was carried out using Kraken2[40] against the Genome Taxonomy Database[41] version 89, which provides equivalent results to Kaiju-determined differences in *C. difficile* abundance as a function of diet phase.

qPCR of human samples. Quantitative PCR was performed on 216 out of 290 samples that were available from the 16S rRNA gene sequencing cohort. qPCR of total 16S rRNA gene copies was carried out in triplicate 10-μl reactions with 200 nM 340F/514R primers using a BioRad CFX384 thermocycler with SYBRSelect for CFX Master Mix (Life Technologies) according to the manufacturer's instructions and an annealing temperature of 60 °C. Absolute quantifications were determined using a standard curve of purified 8F/1542R amplified *Escherichia coli* MG1655 DNA[42]. Reactions were performed in triplicate and mean values were taken for further downstream analyses. Absolute bacterial abundance was derived by adjusting for dilutions during DNA extraction, normalization, and PCR reaction preparation and dividing by the total faecal mass used for DNA extraction in grams.

Bile acid quantification. Human faecal samples were thawed at 4 °C and 25 mg was added to 1 ml of pre-cooled (−20 °C) methanol (containing 0.5 μM deuterated internal standards). Samples were homogenized and then subjected to three cycles of freeze–thaw in liquid nitrogen. Samples were centrifuged (4 °C, 15 min, maximum speed) and 200 μl of the supernatant was transferred to autosampler vials for liquid chromatography and tandem mass spectrometry (LC-MS/MS) analysis. Faecal bile acids were quantified using an ACQUITY ultraperformance liquid-chromatography (UPLC) system coupled with a Xevo TQ-S triple-quadrupole mass spectrometer (Waters, Milford, MA) equipped with an electrospray ionization (ESI) source operating in negative ionization mode as described[43]. Selected ion recording (SIR; *m/z*), multiple reaction monitoring (MRM) transitions, and retention time were developed by running individual bile acid standards. A standard curve was plotted for each individual bile acid for quantification purposes.

SCFA and BCAA quantification. SCFAs and BCAAs were quantified using an Agilent 7890A gas chromatograph coupled with an Agilent 5975 mass spectrometer (Agilent Technologies Santa Clara, CA) using a propyl esterification method as previously described[44,45]. Approximately 25-mg fresh human faecal samples were mixed with 1 ml of 0.005 M NaOH (containing 10 μg/ml internal standard caproic acid-6,6,6-d3), homogenized thoroughly with 1.0-mm-diameter zirconia/silica beads (BioSpec, Bartlesville, OK) and centrifuged (13,200g, 4 °C, 20 min). Supernatant (500 μl) was collected and mixed with an aliquot of 500 μl 1-propanol/pyridine (v/v = 3/2), then 100 μl propyl chloroformate was added following a brief vortex for 1 min. Samples were incubated at 60 °C for 1 h. The derivatized samples were extracted by two-step hexane extraction as described[45]. We added 300 μl hexane to samples followed by centrifugation (2,000g, 4 °C, 5 min) and transfer of 300 μl of the upper layer to an autosampler vial. Another 200 μl hexane was added to samples and the additional 200 μl upper layer was transferred and combined with the first extraction. A total 500 μl volume of extracts was obtained for gas chromatograph–mass spectrometry (GC-MS) analysis. A standard curve was drafted for each analyte to quantify biological concentration in human faecal samples.

Animal experiments

Mice and housing. All experiments, with the exception of the median four weight losers (Extended Data Fig. 4h–j), were conducted at UCSF and approved by the University of California, San Francisco Institutional Animal Care and Use Committee with the support of the UCSF Gnotobiotic Core Facility. Germ-free C57BL/6J mice aged 10–15 weeks were used for transplantation experiments. Mice were bred in-house in a sterile breeding isolator (Class Biologically Clean, USA) and transferred to an experimental isolator one week before experimental procedures. In all experiments, mice were fed a standard autoclaved chow diet ad libitum (Lab Diet 5021) with free access to water at room temperature of 24 ± 1 °C, room humidity 30–70%, and a 12/12-h light/dark cycle (7:00 AM–7:00 PM). Baseline sterility was determined using aerobic and anaerobic culture on multiple rich media and quantitative dual-dye probe qPCR targeting the V6 region of the 16S rRNA gene. Mice were singly housed with environmental enrichment in duplex cages in all experiments except for the pilot transplantation experiment (Fig. 2) and median four weight losers (Extended Data Fig. 4h–j). The total mice per cage in these experiments ranged from 2 to 4 with total mice per group ranging from 3 to 13 as identified in Extended Data Figs. 3b, 4, 6a, 7a, 8a.

The median four weight losers experiment was conducted at the Center for Cardiovascular Research at the Charité in Berlin, Germany. The experiments were performed in accordance with the terms of the German Animal Protection Law, as well as according to international animal welfare legislation and institutional ethical guidelines of the Charité Berlin, Germany, and were approved by the Landesamt für Gesundheit und Soziales (approval number G 0085/17, LAGeSo Berlin, Germany). GF C57BL/6J mice aged 10–18 weeks were used for transplantation experiments. Mice were bred in-house in a sterile breeding isolator (North Kent Plastic, Great Britain) and transferred to an experimental isolator one week before experimental procedures. Mice were fed a standard autoclaved chow diet ad libitum with free access to water at room temperature of 24 ± 1 °C and a 12/12-h light/dark cycle (7:00 AM–7:00 PM). Baseline sterility was determined using aerobic and anaerobic culture on multiple rich media. Mice were housed at 2–4 per cage. Where multiple pre-colonization weight measurements were available for animal experiments, weight loss was normalized to their average. Mice were allocated among treatment groups, balancing age and baseline weight where possible. Blinding of treatment groups was not performed.

Article

Colonization. Samples from multiple individuals were pooled, normalizing 16S rRNA gene copies per g faeces, as identified via qPCR as above, across individuals. Each faecal sample was thawed and prepared in an anaerobic chamber. A total of 1 g faecal matter was removed and diluted with 10 ml sterile 0.9% saline with added cysteine (0.05% w/v). Each diluted sample was then vortexed for 1 min and centrifuged at 5,000 rpm for 1 min or passed through a 100-µm mesh strainer. The resulting preparation was externally sterilized and transferred into gnotobiotic isolators wherein 200 µl was administered by oral gavage. Where spores were co-administered, they were inoculated at 1×10^4 spores per 200 µl gavage. Spores were prepared by plating a lawn of *C. difficile* on brain heart infusion-supplemented with 1% w/v yeast extract (BHIS) medium and incubating it for 7 days at 37 °C under anaerobic conditions. Plates were then washed in PBS and the resulting solution was refrigerated overnight in aerobic conditions. The preparation was then washed 3× in PBS and heated to 70 °C for 20 min to remove any surviving vegetative cells. Spores were enumerated under anaerobic conditions on *C. difficile* selective agar (BD) and visualized using phase contrast microscopy to verify the purity of spores.

Metabolic profiling. Oral glucose tolerance tests were performed by fasting mice for 6 h and then administering 2 mg/kg glucose by oral gavage. Blood glucose was measured at 0, 15, 30, 60, and 120 min after gavage using a OneTouch Ultra 2 (LifeScan, USA). Body fat was measured by either EchoMRI for whole-body fat composition, or dissection and weighing of the epididymal fat pad. Food and water intake were measured for individual mice longitudinally at each time point by collecting body mass (in experiments using singly housed cages), or for the cage in aggregate (for experiments involving cohousing). In the pilot faecal transplantation experiment (Fig. 2), food consumption was measured at days 7–10, 10–14, 14–18 and 18–20. For this experiment, food intake per mouse per day was calculated as follows: [total food intake per cage]/[mice per cage]/[days of food consumption]. Caloric intake was determined by converting to kcal using the value 4.62 kcal/g gross energy for Lab Diet 5021. To measure faecal energy content, faecal pellets were collected from individual mice and lyophilized for 24 h before determination of energy content via bomb calorimetry. After completion of the drying process, the dried masses of the pellets were recorded. Gross energy content was measured using an isoperibol oxygen bomb calorimeter with a semimicro oxygen bomb (Models 6200 and 1109, respectively, from Parr Instrument Co). The calorimeter energy equivalent factor was determined using benzoic acid standards. Sample dropouts occurred due to misfire and were accounted for by using linear mixed models for statistical analysis.

Histology. Proximal colon samples were transferred to cassettes and preserved overnight in 10% neutral buffered formalin before being transferred to ethanol and stored at 4 °C. Samples were subsequently embedded in paraffin, sectioned (4 µm), and stained with haematoxylin and eosin (H&E). Slides were blindly scored according to the methodology of Erben et al.[46].

16S rRNA gene sequencing and analysis. DNA samples were extracted from 48 mouse faecal samples via bead beating for 4 min (Min-Beadbeater-24, BioSpec), using Lysing Matrix E (MPBio) and the lysis buffer of a Wizard SV 96 Genome DNA kit (Promega) with subsequent DNA isolation according to the manufacturer's protocol. Amplification was conducted by combining 2 µl DNA with 25 µl AmpliTaq Gold 360 Master Mix (Life Technologies), 5 µl of primers (2 µM each GoLay-barcoded 515/806R), and 18 µl H_2O. Amplification was as follows: 10 min 95 °C, 30× (30 s 95 °C, 30 s 50 °C, 30 s 72 °C), and 7 min 72 °C. Data were processed as described above for the MMS human cohort.

Time-course analysis of the mouse experiment was carried out using ZIBR v0.1[47] including random effects to account for repeated sampling across time using the Benjamin–Hochberg corrected joint Q value, unless 0 values comprised >90% or <10% for the given feature, in which case only the logistic or beta component was considered, respectively. For plotting purposes, $\log_2$(fold-change) was considered as the difference in median CLR-normalized abundance. Gene content based on 16S rRNA gene sequencing data was inferred using PICRUSt v1.0.0 based on closed reference OTU assignments to the Greengenes May 2013 release using QIIME v1.9.1. These were compared via linear mixed effect model as before with mouse as a random effect, with FDR $Q < 0.1$ considered as statistically significant. KEGG Pathway enrichment was carried out using clusterProfiler v3.4.1. Engraftment of ASVs from the pooled human sample (Fig. 2a) was quantified at 36% and 52% for pre- and post-diet recipient groups, respectively, and 66% and 83% at the genus level in line with previous reports[48,49].

C. difficile testing, quantification, and isolation. Direct culture was carried out using BBL *Clostridium difficile* selective agar (CDSA; Becton, Dickson and Company). Samples were thawed in an anaerobic chamber (Coy Lab Products) and ~10 mg faeces was directly applied to agar using a four-quadrant streak method. Plates were incubated for 72 h at 37 °C in 5% CO_2, 10% H_2, and 85% N_2. Plates were then removed from anaerobic conditions and imaged under normal and long-wave UV light. Positive specimens were determined by the presence of at least one colony fitting the *C. difficile* morphology: yellow, ground-glass, slightly filamentous edges with fluorescence under long-wave UV light. ELISA was carried out using a commercial kit according to the manufacturer's instructions (TGC-E001-1, tgcBiomics) to detect both TcdA and TcdB toxins with detection limits of 0.5 and 1 ng/ml, respectively. Endpoint PCR for *tcdA* and *tcdB* was carried out using a multiplexed assay according the protocol of Persson, Torpdahl, and Olsen[50] excluding the 16S rRNA gene primer set of the 5-plex on previously sequenced DNA extracted with the modified Promega approach above. *C. difficile* and *tcdB* were quantified via qPCR using the following oligonucleotides[51]: 5-GCAAGTTGAGCGATTTACTTCGGT-3 ($P_{CD\text{-forward}}$), 5-GTACTGGCTCACCTTTGATATTYAAGAG-3 ($P_{CD\text{-reverse}}$), 5-[6FAM]TGCCTCTCAAATATATTATCCCGTATTAG[BHQ1]-3 ($P_{CD\text{-probe}}$), and 5-TACAAACAGGTGTATTTAGTACAGAAGATGGA-3 ($P_{tcdB\text{-forward}}$), 5-CACCTATTTGATTTAGMCCTTTAAAAGC-3 ($P_{tcdB\text{-reverse}}$), 5-[HEX]TTTKCCAGTAAAATCAATTGCTTC[BHQ1]-3 ($P_{tcdB\text{-probe}}$).

qPCR was conducted using iTaq Universal Probes Supermix (BioRad) according to the manufacturer's instructions with an annealing temperature of 56.6 °C with a CFX384 thermocycler (BioRad). The limit of detection was estimated to be 1×10^3 genome equivalents per g on the basis of extraction of a dilution series of *C. difficile* JBZPo1. Remaining aliquots of 61 human faecal samples were assayed using the Cepheid Xpert C.diff-Epi assay version 2 at the UCSF Clinical Microbiology lab. All assayed samples tested negative for Toxin B, Binary Toxin, and TcdC, including those that had previously been assayed positive via ELISA, qPCR, and culture. Sample remnants were then subjected to an enrichment culture algorithm by incubating for 72 h at 37 °C in CCMB-TAL (Anaerobe Systems) with ELISA performed for TcdA/B as above on supernatants after 48 h and 72 h. qPCR with the above primers and probes was carried out after 72 h with DNA extracted using the ZymoBIOMICS 96 MagBead DNA kit according to the manufacturer's protocol. After 48 h, CCMB-TAL was subcultured onto CDSA and representative colonies were subcultured and their 16S rRNA sequence determined (GeneWiz Sequencing). A total of 18 samples were presumptively positive on the basis of culture morphologies consistent with *C. difficile*; however, after sequencing these were primarily determined to represent *Clostridium innocuum*. One sample contained a genuine *C. difficile* isolate (MMSP50 CONVD time point) and no isolate could be obtained from the previously ELISA-positive sample (MMSP30 CONVD time point). ELISA and qPCR of enriched cultures confirmed this result with no detectable toxin A/B or amplicon, respectively.

C. difficile JBZPo1 and genetic characterization. Metagenomic sequencing of faecal DNA from a subset of recipient mice (Fig. 2a, Supplementary Table 3), was performed. Libraries were prepared using the Nextera XT protocol according to the manufacturer's instructions and sequenced by Illumina NovaSeq with paired end 140 × 140 reads obtaining 0.56–16.10 Gb per sample. To generate a draft assembly of the potential causative *C. difficile* strain, a cross-assembly was created from all samples within the post-diet recipient mice (Megahit[52]), and then these assemblies were used to generate metagenome assembled genomes (MAGs) using composition and abundance across samples[53]. A total of 204 MAGs were assigned taxonomy using MetaWrap[54] and a single *C. difficile* genome was recovered with an estimated 96.66% completion with 0.43% contamination on the basis of single-copy marker genes[55]. A sequencing library was prepared from gDNA of the JBZPo1 isolate using the Nextera XT protocol according to the manufacturer's instructions (Illumina) and sequenced using paired end 251 × 251 reads (V3 MiSeq chemistry) with a total of 2,780,073 reads after demultiplexing. Reads were filtered using Trimmomatic[56] and assembled using SPAdes 3.11.1[57]. The resulting assembly was submitted to NCBI PGAP for annotation. Comparison of JBZPo1 to the *C. difficile* MAG was conducted using pyani[58], which gave a whole-genome average nucleotide identity of >99.9%. This genome was placed in a phylogenetic tree using Phylophlan[59] using available *C. difficile* genomes retrieved from the PATRIC[60] with ribotypes retrieved based on literature review. The presence of *tcdA*, *tcdB*, *cdtR*, *cdtA*, and *cdtB* was determined using BLAST. Multilocus sequence typing was performed with mlst (https://github.com/tseemann/mlst).

Statistical analysis

All statistics were carried out in R version 3.4.0 or 3.6.1 using Welch's *t*-tests or Wilcoxon rank sum and signed rank tests where appropriate unless otherwise indicated. For non-microbiome-related analyses, linear mixed effects models (LMMs) were performed using lmerTest[61] with multiple testing corrections via the ghlt function of multcomp using Tukey's all-pair comparison method. For non-normally distributed variables, a Kruskal–Wallis test followed by Dunn's post hoc test was performed as implemented with the dunn.test package in R (version 1.3.5). Graphical representation was carried out using ggplot2 unless otherwise stated[62]. Values are presented as mean ± s.e.m. unless otherwise noted. In boxplots, the centre line represents the median with the limits representing the first and third quartiles, whiskers extending up to 1.5× IQR and outliers shown as individual points when all points have not been plotted (*n* < 10). For analysis of weight changes in mice, weights were normalized to the average of run-in samples where available to calculate the percentage change in body weight and carried forward for statistical analysis. Area under the curve was calculated as either the total area under the curve (AUC) using the trapezoid rule, or the incremental AUC (iAUC) as described[63].

Reporting summary

Further information on research design is available in the Nature Research Reporting Summary linked to this paper.

Data availability

16S rRNA gene and metagenomic sequencing reads have been deposited in the SRA under BioProject PRJNA412411. The genome of *C. difficile* JBZPo1 has been deposited under BioProject PRJNA503906. The following public databases were used: The Genome Taxonomy Database (https://gtdb.ecogenomic.org/), DADA2 Taxonomic Training Sets (http://benjjneb.github.io/dada2/assign.html), CAZy (http://www.cazy.org/), and KEGG (https://www.genome.jp/kegg/). Source data are provided with this paper.

27. Caporaso, J. G. et al. Ultra-high-throughput microbial community analysis on the Illumina HiSeq and MiSeq platforms. *ISME J.* **6**, 1621–1624 (2012).
28. Callahan, B. J. et al. DADA2: High-resolution sample inference from Illumina amplicon data. *Nat. Methods* **13**, 581–583 (2016).
29. Wang, Q., Garrity, G. M., Tiedje, J. M. & Cole, J. R. Naive Bayesian classifier for rapid assignment of rRNA sequences into the new bacterial taxonomy. *Appl. Environ. Microbiol.* **73**, 5261–5267 (2007).
30. Fernandes, A. D., Macklaim, J. M., Linn, T. G., Reid, G. & Gloor, G. B. ANOVA-like differential expression (ALDEx) analysis for mixed population RNA-seq. *PLoS ONE* **8**, e67019 (2013).
31. Fernandes, A. D. et al. Unifying the analysis of high-throughput sequencing datasets: characterizing RNA-seq, 16S rRNA gene sequencing and selective growth experiments by compositional data analysis. *Microbiome* **2**, 15 (2014).
32. Langmead, B. & Salzberg, S. L. Fast gapped-read alignment with Bowtie 2. *Nat. Methods* **9**, 357–359 (2012).
33. Kanehisa, M., Goto, S., Sato, Y., Furumichi, M. & Tanabe, M. KEGG for integration and interpretation of large-scale molecular data sets. *Nucleic Acids Res.* **40**, D109–D114 (2012).
34. Zhao, Y., Tang, H. & Ye, Y. RAPSearch2: a fast and memory-efficient protein similarity search tool for next-generation sequencing data. *Bioinformatics* **28**, 125–126 (2012).
35. Nayfach, S. & Pollard, K. S. Average genome size estimation improves comparative metagenomics and sheds light on the functional ecology of the human microbiome. *Genome Biol.* **16**, 51 (2015).
36. Law, C. W., Chen, Y., Shi, W. & Smyth, G. K. voom: precision weights unlock linear model analysis tools for RNA-seq read counts. *Genome Biol.* **15**, R29 (2014).
37. Wu, D. et al. ROAST: rotation gene set tests for complex microarray experiments. *Bioinformatics* **26**, 2176–2182 (2010).
38. Buchfink, B., Xie, C. & Huson, D. H. Fast and sensitive protein alignment using DIAMOND. *Nat. Methods* **12**, 59–60 (2015).
39. Menzel, P., Ng, K. L. & Krogh, A. Fast and sensitive taxonomic classification for metagenomics with Kaiju. *Nat. Commun.* **7**, 11257 (2016).
40. Wood, D. E., Lu, J. & Langmead, B. Improved metagenomic analysis with Kraken 2. *Genome Biol.* **20**, 257 (2019).
41. Chaumeil, P.-A., Mussig, A. J., Hugenholtz, P. & Parks, D. H. GTDB-Tk: a toolkit to classify genomes with the Genome Taxonomy Database. *Bioinformatics* **36**, 1925–1927 (2019).
42. Edwards, U., Rogall, T., Blöcker, H., Emde, M. & Böttger, E. C. Isolation and direct complete nucleotide determination of entire genes. Characterization of a gene coding for 16S ribosomal RNA. *Nucleic Acids Res.* **17**, 7843–7853 (1989).
43. Sarafian, M. H. et al. Bile acid profiling and quantification in biofluids using ultra-performance liquid chromatography tandem mass spectrometry. *Anal. Chem.* **87**, 9662–9670 (2015).
44. Cai, J. et al. Orthogonal comparison of GC-MS and ¹H NMR spectroscopy for short chain fatty acid quantitation. *Anal. Chem.* **89**, 7900–7906 (2017).
45. Zheng, X. et al. A targeted metabolomic protocol for short-chain fatty acids and branched-chain amino acids. *Metabolomics* **9**, 818–827 (2013).
46. Erben, U. et al. A guide to histomorphological evaluation of intestinal inflammation in mouse models. *Int. J. Clin. Exp. Pathol.* **7**, 4557–4576 (2014).
47. Chen, E. Z. & Li, H. A two-part mixed-effects model for analyzing longitudinal microbiome compositional data. *Bioinformatics* **32**, 2611–2617 (2016).
48. Turnbaugh, P. J. et al. The effect of diet on the human gut microbiome: a metagenomic analysis in humanized gnotobiotic mice. *Sci. Transl. Med.* **1**, 6ra14 (2009).
49. Fouladi, F. et al. Sequence variant analysis reveals poor correlations in microbial taxonomic abundance between humans and mice after gnotobiotic transfer. *ISME J.* **14**, 1809–1820 (2020).
50. Persson, S., Torpdahl, M. & Olsen, K. E. New multiplex PCR method for the detection of *Clostridium difficile* toxin A (tcdA) and toxin B (tcdB) and the binary toxin (cdtA/cdtB) genes applied to a Danish strain collection. *Clin. Microbiol. Infect.* **14**, 1057–1064 (2008).
51. Kubota, H. et al. Longitudinal investigation of carriage rates, counts, and genotypes of toxigenic *Clostridium difficile* in early infancy. *Appl. Environ. Microbiol.* **82**, 5806–5814 (2016).
52. Li, D., Liu, C.-M., Luo, R., Sadakane, K. & Lam, T.-W. MEGAHIT: an ultra-fast single-node solution for large and complex metagenomics assembly via succinct de Bruijn graph. *Bioinformatics* **31**, 1674–1676 (2015).
53. Alneberg, J. et al. Binning metagenomic contigs by coverage and composition. *Nat. Methods* **11**, 1144–1146 (2014).
54. Uritskiy, G. V., DiRuggiero, J. & Taylor, J. MetaWRAP—a flexible pipeline for genome-resolved metagenomic data analysis. *Microbiome* **6**, 158 (2018).
55. Parks, D. H., Imelfort, M., Skennerton, C. T., Hugenholtz, P. & Tyson, G. W. CheckM: assessing the quality of microbial genomes recovered from isolates, single cells, and metagenomes. *Genome Res.* **25**, 1043–1055 (2015).
56. Bolger, A. M., Lohse, M. & Usadel, B. Trimmomatic: a flexible trimmer for Illumina sequence data. *Bioinformatics* **30**, 2114–2120 (2014).
57. Bankevich, A. et al. SPAdes: a new genome assembly algorithm and its applications to single-cell sequencing. *J. Comput. Biol.* **19**, 455–477 (2012).
58. Pritchard, L., Glover, R. H., Humphris, S., Elphinstone, J. G. & Toth, I. K. Genomics and taxonomy in diagnostics for food security: soft-rotting enterobacterial plant pathogens. *Anal. Methods* **8**, 12–24 (2015).
59. Segata, N., Börnigen, D., Morgan, X. C. & Huttenhower, C. PhyloPhlAn is a new method for improved phylogenetic and taxonomic placement of microbes. *Nat. Commun.* **4**, 2304 (2013).
60. Wattam, A. R. et al. Improvements to PATRIC, the all-bacterial Bioinformatics Database and Analysis Resource Center. *Nucleic Acids Res.* **45**, D535–D542 (2017).
61. Kuznetsova, A., Brockhoff, P. B. & Christensen, R. H. B. lmerTest package: tests in linear mixed effects models. *J. Stat. Softw.* **82**, 1–26 (2017).
62. Wickham, H. *ggplot2: Elegant Graphics for Data Analysis* (Springer, 2016).
63. Brouns, F. et al. Glycaemic index methodology. *Nutr. Res. Rev.* **18**, 145–171 (2005).

Article

Extended Data Fig. 1 | MMS diet intervention study. a, CONSORT diagram describing enrolment, allocation, and data analysis. **b**, Per time point group sizes and timing of data collection. Participants in the diet group underwent 2 months of a very-low calorie liquid diet followed by an additional month of a conventional low-calorie diet. During the fourth month, they were instructed to maintain a stable weight. During all diet periods individuals were counselled by clinical nutritionists. Time points with data collection are shown for both diet and control participants. **c, e**, Daily consumption of macronutrients measured by mass (**c**) and percentage of daily energy intake (**e**) in diet group ($n_{baseline} = 34$, $n_{VLCD} = 34$, $n_{CONVD} = 30$, $n_{MAINT} = 32$ participants). **d**, Total daily caloric

intake during diet phases ($n_{intervention}$ as in **c**, **e**, control group $n_{baseline} = 30$, $n_{CONVD} = 22$, $n_{MAINT} = 24$ participants). **f**, Decreases in relative body fat are observed in the intervention group ($n_{baseline} = 40$, $n_{CONVD} = 36$, $n_{MAINT} = 33$ participants) relative to the control group ($n_{baseline} = 40$, $n_{CONVD} = 24$, $n_{MAINT} = 26$ participants). **g**, Diet leads to improvement in glucose tolerance as measured by OGTT within and between diet ($n_{baseline} = 40$, $n_{CONVD} = 36$, $n_{MAINT} = 35$ participants) and control ($n_{baseline} = 40$, $n_{CONVD} = 25$, $n_{MAINT} = 26$ participants) groups. LMM with Tukey's two-sided all-pair comparison. In boxplots: centre line, median; box, first and third quartiles; whiskers, 1.5× interquartile range (IQR) with outliers individually plotted.
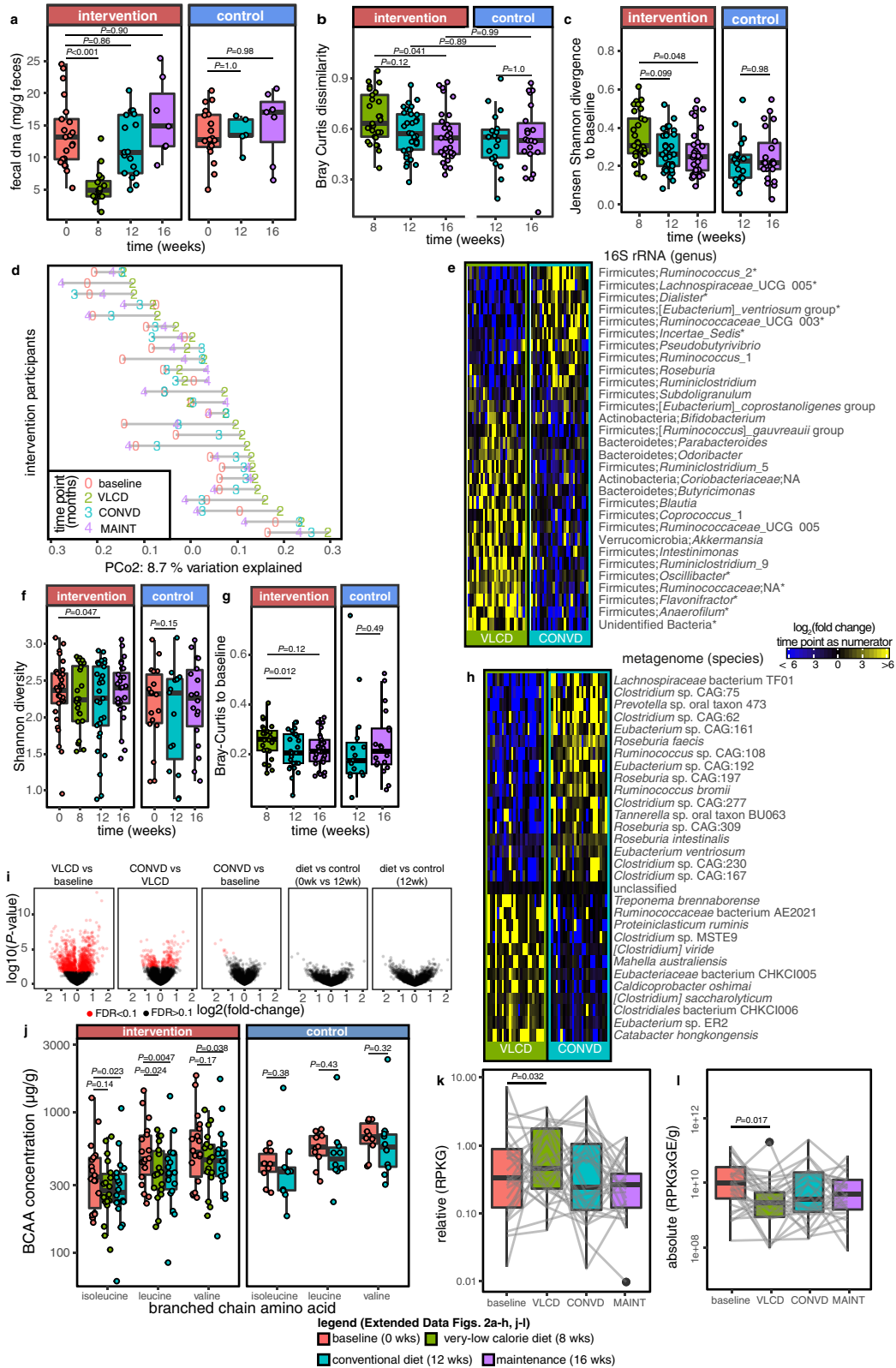
Extended Data Fig. 2 | See next page for caption.

Extended Data Fig. 2 | Reproducible and reversible shifts are observed in the gut microbiota as a result of caloric restriction in both 16S rRNA amplicon and shotgun metagenomic sequencing data. a, Concentration of faecal DNA reveals decreased microbiota abundances in response to VLCD contrasting within diet group ($n_{baseline}$ = 21, n_{VLCD} = 16, n_{CONVD} = 17, n_{MAINT} = 7 participants) and between diet and control groups ($n_{baseline}$ = 19, n_{CONVD} = 5, n_{MAINT} = 7 participants). Microbiota determined by 16S rRNA gene sequencing revert to a state more closely resembling baseline samples after VLCD (n = 19–33 per group per time point; Supplementary Table 3) by both Bray–Curtis dissimilarity (**b**) and Jensen Shannon divergence (**c**; also $P < 0.001$, R^2 = 0.031 by ADONIS with Participant ID as stratum). **d**, Reproducible shifts in community membership are observed across individuals on the second principal coordinate in response to diet followed by reversion during conventional diet and maintenance (Unweighted UniFrac). Each series of connected points represents a single individual in the study with the number representing the time point of the study in months. **e**, Genera whose abundances were altered by VLCD demonstrate rapid reversion during the conventional diet (30 most important genera by GINI coefficient displayed, Random Forest, *FDR Q < 0.1 ALDEx2). **f**, Shannon diversity is significantly decreased after conventional diet (P = 0.047, n = 29, mean difference = 0.149 (0.002–0.296 95% CI), paired Welch's two-sided t-test). **g**, Microbiota revert to a state more closely resembling baseline samples after VLCD, as measured through species-level metagenomic assignments (P = 0.012, n = 15–29 per group per time point; Supplementary Table 3, two-sided Wilcoxon signed rank test). **h**, Metagenomic species whose abundances are altered by VLCD demonstrate rapid reversion during the conventional diet and maintenance phases (30 most important genera by GINI coefficient displayed). **i**, Volcano plots of differentially abundant KOs by contrast in metagenome data. VLCD demonstrates the largest effect size with apparent reversion when contrasted against CONVD. Effects of CONVD compared to baseline and cross-group comparisons yield minimal significant results. Statistical analysis was conducted using Limma. **j**, The BCAAs leucine and isoleucine are significantly reduced during VLCD ($n_{intervention}$ = 18, $n_{control}$ = 10 participants per time point, Wilcoxon signed-rank test). **k**, The butanoyl-CoA:acetoacetate CoA-transferase α-subunit, an enzyme that catalyses the final step in the production of butyrate, is increased in relative abundance during VLCD (FDR Q = 0.032, Limma; Supplementary Table 4). **l**, Normalizing relative abundance of butanoyl-CoA:acetoacetate CoA-transferase with qPCR quantification of 16S rRNA gene copies to infer the absolute number of genome equivalents (GE) in the sample demonstrates a decrease in the absolute abundance of the enzyme family (P = 0.017, LMM with Tukey two-sided all-pair comparison). Sample size in number of participants for **k**, **l**: $n_{baseline}$ = 29, n_{VLCD} = 24, n_{CONVD} = 29, n_{MAINT} = 28. In boxplots: centre line, median; box, first and third quartiles; whiskers, 1.5× interquartile range (IQR) with outliers individually plotted.
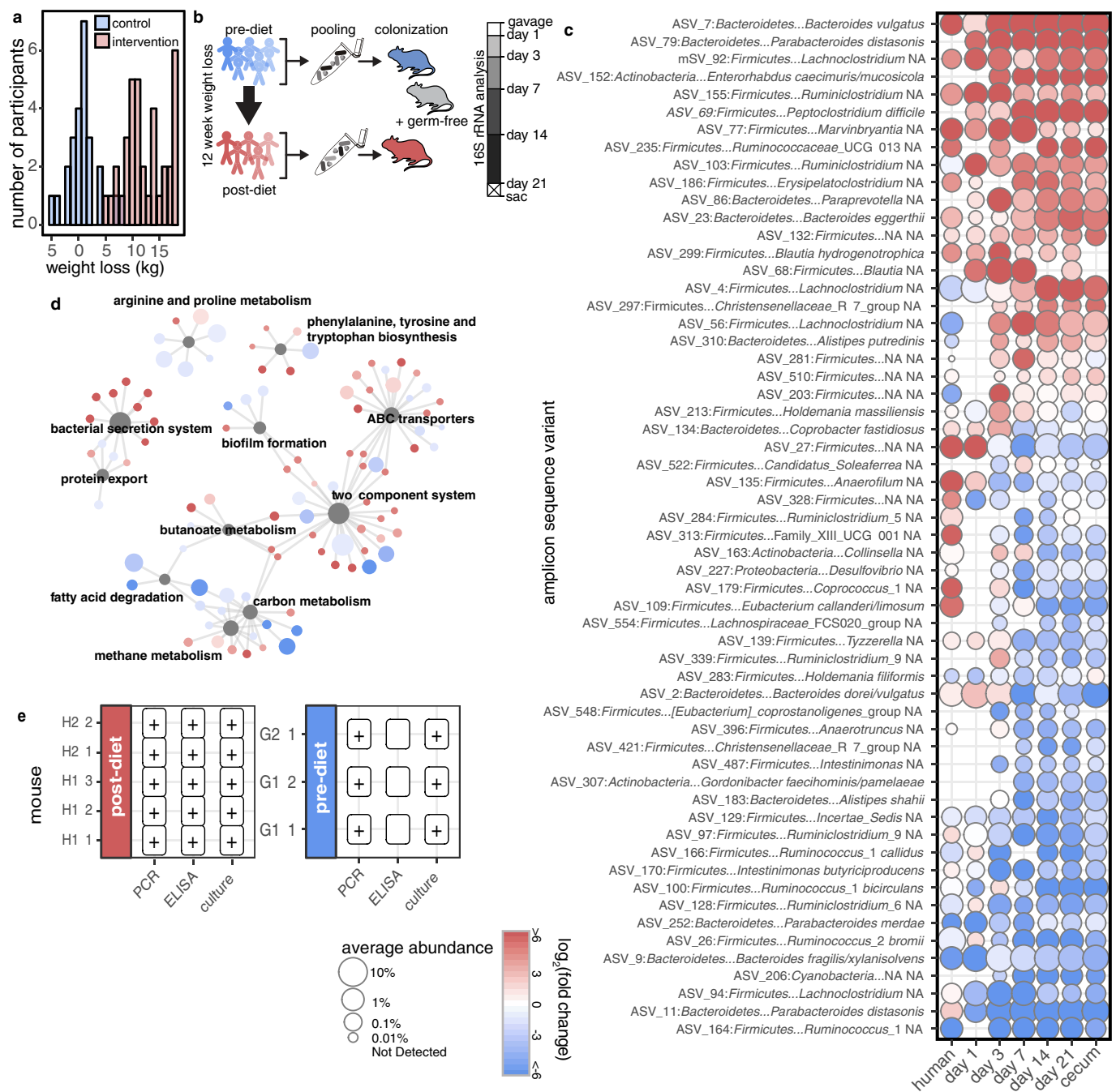
Extended Data Fig. 3 | Diet-dependent changes in the microbiome are maintained following transplantation to GF mice. a, Distribution of weight loss in diet intervention participants identified the five individuals that lost the most weight for transplantation of stool samples to GF C57BL/6J mice. **b**, Experiment design and microbiota sampling times. **c**, Differential 16S rRNA ASV abundances in human donors and recipient mice demonstrate 58 candidate effectors of the weight-loss phenotype (zero-inflated beta regression model with random effects (ZIBR), FDR Q < 0.1, Supplementary Table 6). Note: taxonomy assigned using SILVA 123 with *Peptoclostridium difficile* synonymous for *C. difficile*. **d**, Functional differences between pre- and post-diet recipient communities by enrichment of KEGG functional pathways based on inferred gene content from amplicon sequencing (PICRUSt, Supplementary Table 7). Comparison of groups predicts altered amino acid, carbohydrate, and SCFA metabolic function. Central nodes represent KEGG pathways significantly enriched by their constituent significant differentially abundant KOs, shown with fold-change (colour) and FDR value (size) indicated (FDR Q < 0.1, LMM). **e**, Detection of *C. difficile* and TcdA/TcdB by endpoint PCR, ELISA, and selective and differential culture demonstrates active toxin production in post-diet mice at time of death.
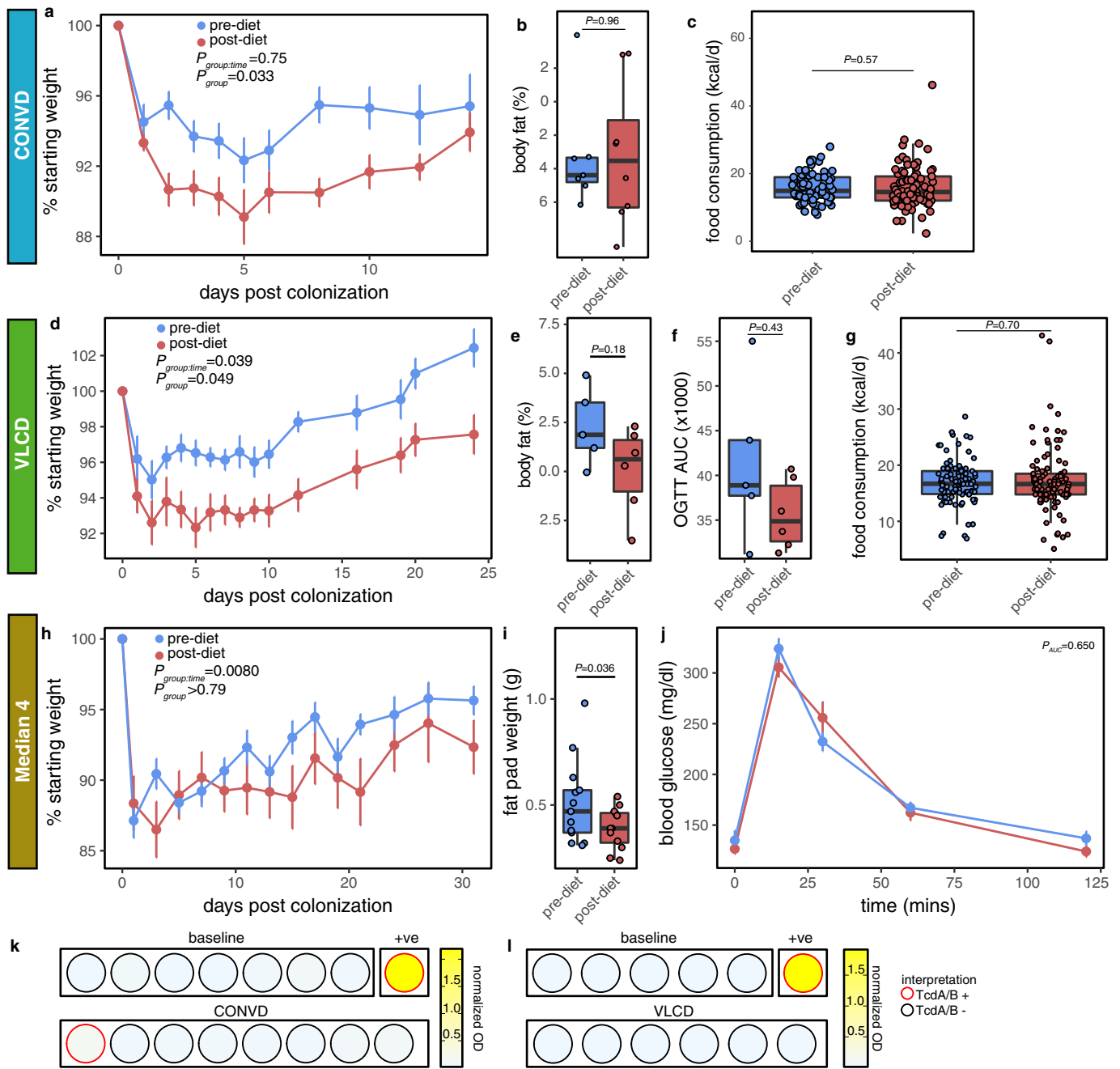
Extended Data Fig. 4 | Replication microbiome transplantation experiments. a, Replication of experiment with transplantation of stool samples from five participants who lost most weight during conventional diet demonstrates significant differences in body weight between mice that received pre-diet and post-diet samples (Fig. 2b); there are no significant differences in body fat (**b**) or food consumption (**c**; $n_{pre-diet}=7$, $n_{post-diet}=8$ mice, LMM). Each point in **c** represents the measurement for a single mouse on a single day. **d**, Transplantation of pooled faecal samples from five participants who lost most weight during VLCD reveals significantly more weight loss in post-diet sample recipient mice (LMM). **e**, **f**, Post-diet recipient mice also show a trend towards reduced body fat (**e**) and improved OGTT (**f**; $P=0.18$ and $P=0.43$ respectively, two-sided Mann–Whitney U test). In **d**–**f**, $n_{pre-diet}=5$, $n_{post-diet}=6$ mice. **g**, Food intake was not significantly different between pre- and post-diet recipient mice over time or between groups ($P=0.70$, LMM $n_{post-diet}=6$,

$n_{pre-diet}=5$ mice measured over 16 time points as in **d**). **h**, **i**, Transplantation of pooled faecal samples from the median four weight losers revealed a small but significant effect on weight gain in recipient mice (**h**; LMM, $n_{pre-diet}=13$, $n_{post-diet}=12$ mice per time point) with an associated reduction in body fat as measured by epididymal fat pad weight (**i**; $P=0.036$, one-tailed Welch's t-test). **j**, This cohort showed no significant differences in OGTT results (AUC, $P=0.650$, two-sided Mann–Whitney U test). Data shown as mean ± s.e.m. where relevant. TcdA/B ELISA demonstrates a lack of stable *C. difficile* colonization in **k** (CONVD) and **l** (VLCD) replication experiments (ELISA reactions shown for individual animals at days 4 and 20 after colonization, respectively). LMM with participant as random effect and Tukey two-sided all-pair comparison unless otherwise noted. In boxplots: centre line, median; box, first and third quartiles; whiskers, 1.5× interquartile range (IQR) with outliers individually plotted.
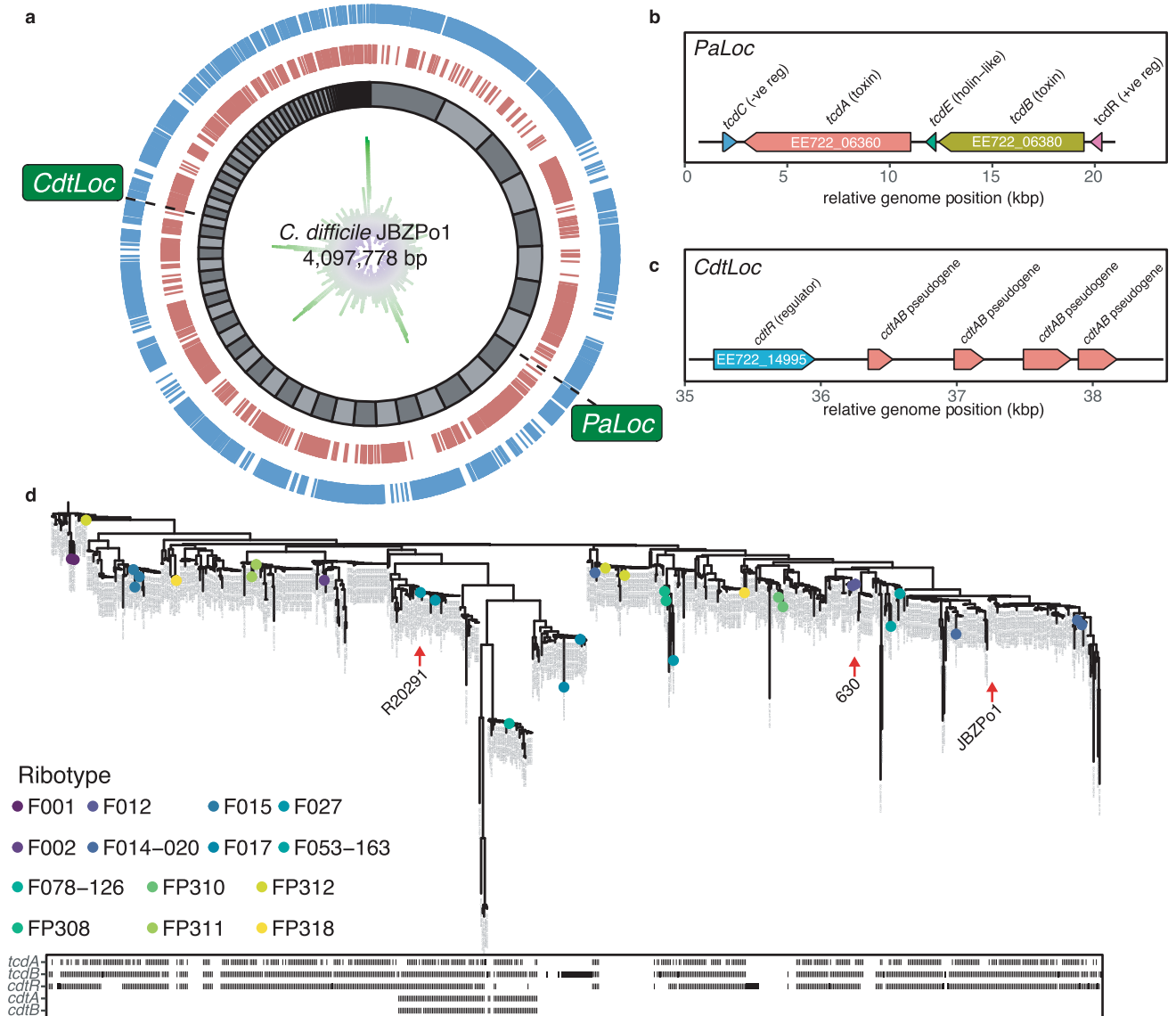
Extended Data Fig. 5 | Characterization of *C. difficile* JBZPo1. a, JBZPo1 was assembled with 255-fold coverage (Illumina MiSeq 250) into 120 contigs (inner grey track; N50 = 87,201 bp) with an average GC content of 28.6% (green–purple centre track showing GC content), and 3,777 coding sequences (outer red and blue tracks displaying positive and negative strands, respectively). **b**, The

C. difficile pathogenicity locus (PaLoc) encodes both toxin A (*tcdA*) and B (*tcdB*). **c**, The binary toxin (*cdt*) locus (CdtLoc) does not encode intact binary toxin. **d**, Phylogenetic tree of 717 *C. difficile* genomes and associated virulence factor carriage places JBZPo1 flanked by Ribotype 014-20 strains and separate from the hypervirulent epidemic NAP1/B1/027 strains (for example, R20291).
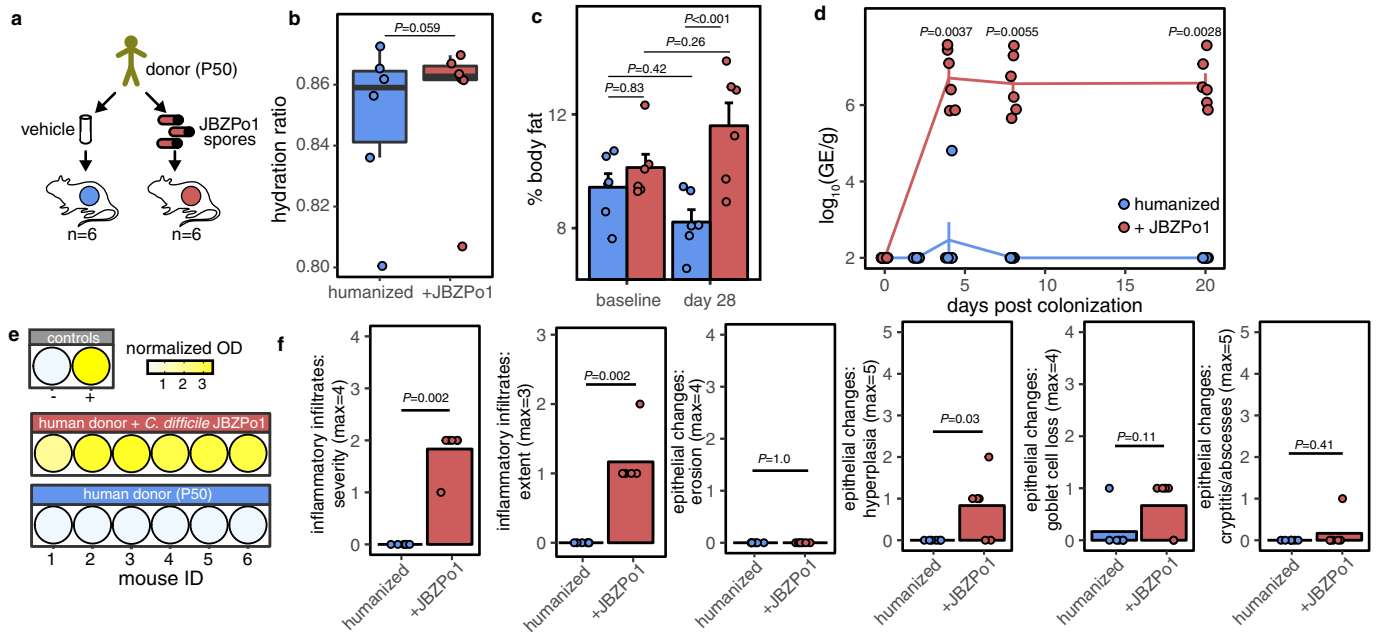
Extended Data Fig. 6 | Extended data relating to *C. difficile* sufficiency experiments. a, Experimental design relating to JBZPo1 transplantation experiment (Fig. 3b). **b**, Establishment of colonization with *C. difficile* JBZPo1 did not lead to dehydration as determined by hydration ratio (hydration ratio = [total body water − free water]/lean mass; *P* = 0.59, two-sided Mann–Whitney *U* test). Centre line, median; box, first and third quartiles; whiskers, 1.5× interquartile range (IQR) with outliers individually plotted. **c**, Body composition analysis revealed a significant difference between humanized vehicle control and *C. difficile* colonized mice at the end of the experiment

(*P* < 0.001, LMM with Tukey's two-sided all-pair comparison, *n* = 6 mice per group), which suggests that *C. difficile* caused increased adiposity. **d**, Quantification of JBZPo1 in recipient mice (*P* = 0.003–0.006, *n* = 6 mice per group per time point except *n* = 5 mice at 8 days in humanized control owing to missing sample; two-sided Mann–Whitney *U* test). Data shown as mean ± s.e.m. **e**, ELISA of caecal contents from recipient mice confirmed production of TcdA/TcdB only in JBZPo1 recipient mice at end of experiment. **f**, Blinded pathological analysis revealed minor neutrophil infiltration with reactive changes (two-sided Mann–Whitney *U* test, *n* = 6 mice per group).
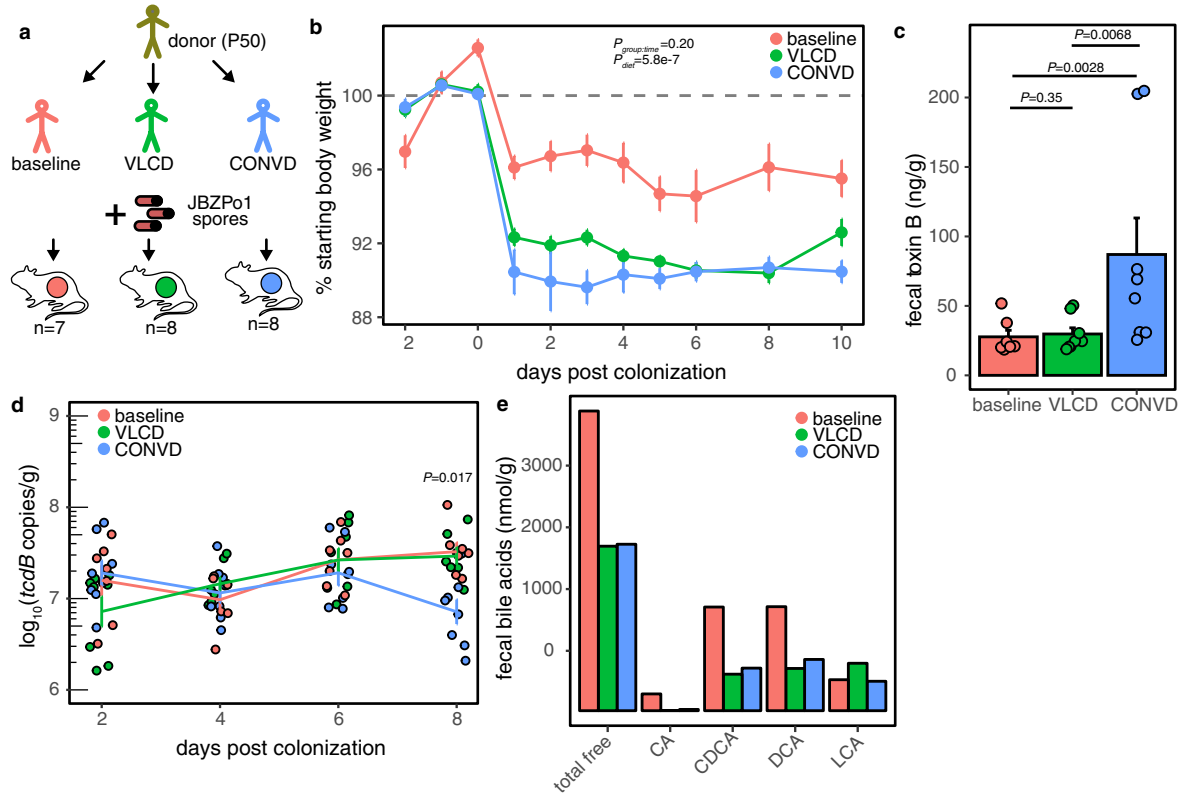
Extended Data Fig. 7 | Diet-induced changes in microbiota influence _C. difficile_-associated weight loss and Toxin B expression. a, Experimental design. **b**, Weight loss over time demonstrates a significant effect of diet of donor ($n = 7$–8 mice per group per day as in **a**; $P = 5.9 \times 10^{-5}$, estimate = -4.6% (-6.6 to -2.7 95% CI) for VLCD, $P = 1.5 \times 10^{-7}$, estimate = -6.6% (-8.5 to -4.6 95% CI) for CONVD). **c**, Mice colonized with stool samples from donors on CONVD showed an increase in TcdB expression over baseline 2 days after colonization ($P = 0.003$, $n = 7$–8 mice per group as in **a**, Kruskal–Wallis with two-sided Dunn's test). **d**, _C. difficile_ carriage did not differ significantly among groups (suggesting no modulation of virulence), with the exception of 8 days after colonization in CONVD-recipient mice ($P = 0.017$ CONVD versus baseline; $n = 7$–8 mice per group as in **a**; two-sided Mann–Whitney _U_ test). Data shown as mean ± s.e.m. in **c**, **d**. **e**, Concentrations of key bile acids in P50 in response to diet ($n = 1$ participant per time point). LMM with participant as random effect and Tukey two-sided all-pair comparison unless otherwise noted.
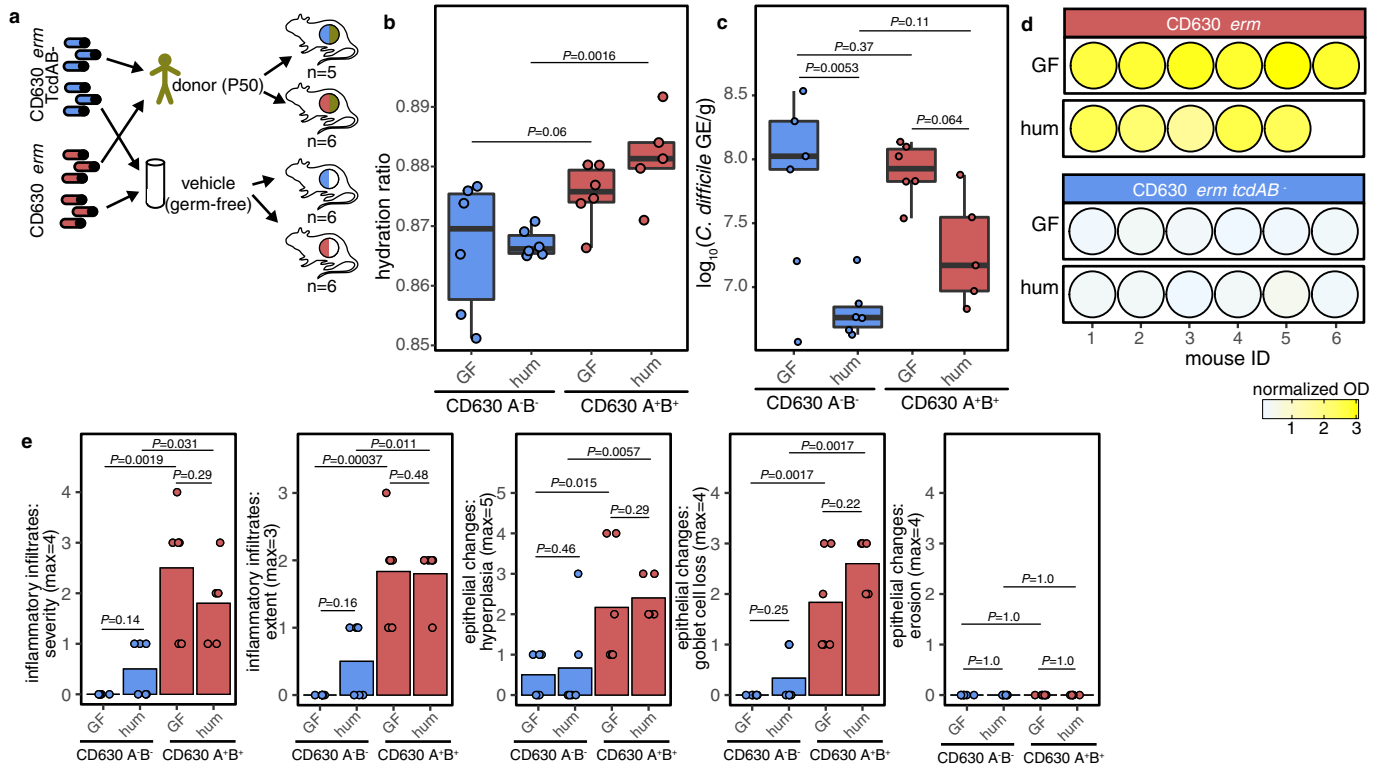
Extended Data Fig. 8 | Extended Data relating to necessity of Toxins A and B in metabolic phenotypes. a, Experimental design relating to *C. difficile* 630 toxin-deficient mutant transplantation experiment (Fig. 3g). **b**, Colonization with TcdA/B⁺ strains does not lead to dehydration in GF animals and increases hydration in humanized animals (*P* = 0.06 and *P* = 0.0016 respectively, Kruskal–Wallis with two-sided Dunn's test). **c**, Caecal *C. difficile* colonization level is not significantly different between strains (*P* = 0.37 and *P* = 0.11 for GF and

humanized mice, respectively, Kruskal–Wallis with two-sided Dunn's test), but is altered in mono-colonization versus humanized mice. **d**, ELISA of caecal contents confirms production of toxin only in *C. difficile* 630 Δ*erm* mutants. **e**, Dense neutrophil and lymphocyte infiltration along with moderate epithelial hyperplasia and goblet cell loss due to TcdA⁺ TcdB⁺ *C. difficile* irrespective of colonization background (Kruskal–Wallis test with two-sided Dunn's post hoc test). In **b**–**e**, *n* = 5–6 mice per group as in **a**.
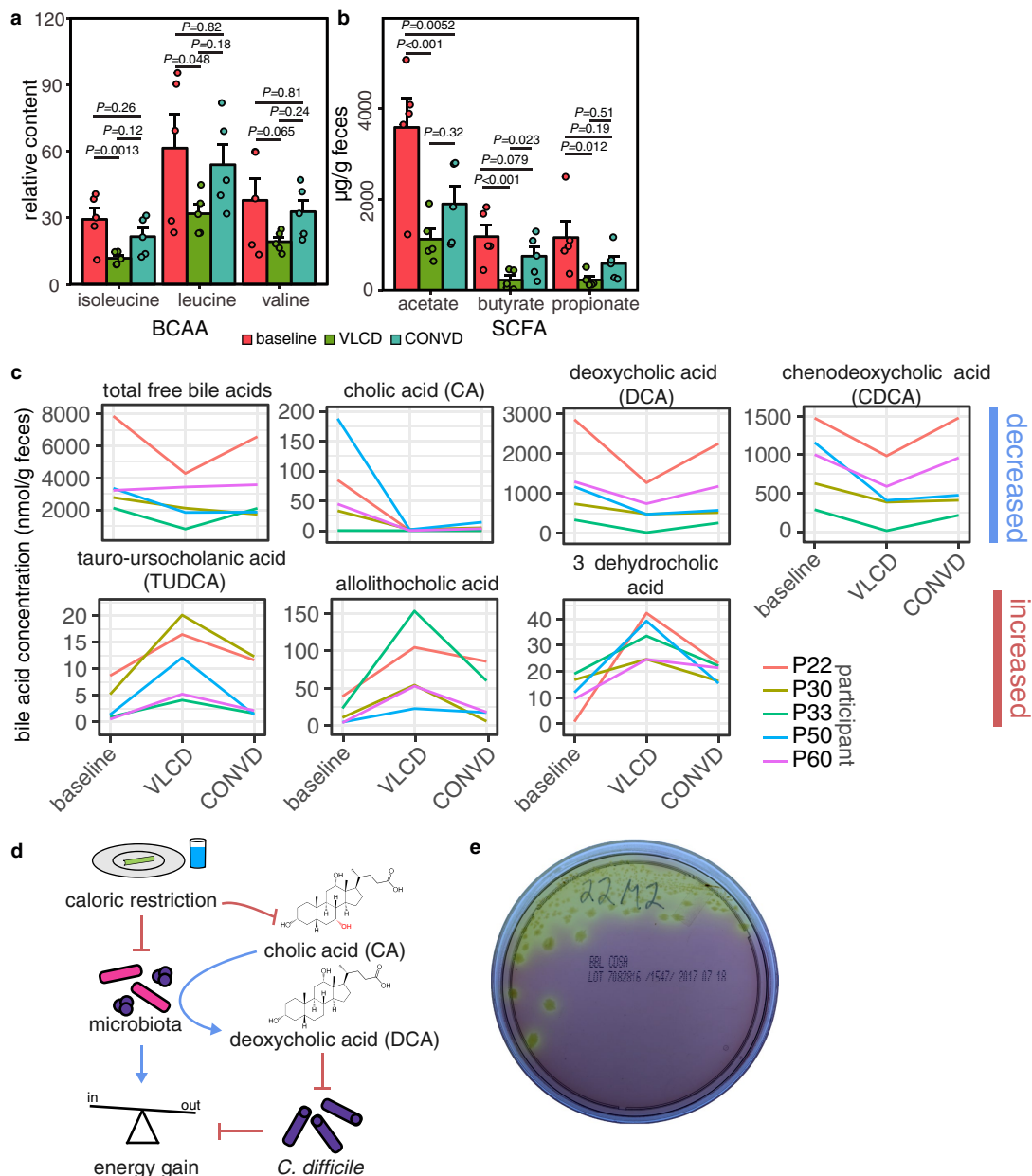
Extended Data Fig. 9 | Metabolomic profiling of the five participants who lost the most weight supports a working model for the effect of caloric restriction on colonization resistance. a, **b**, BCAAs (**a**) and SCFAs (**b**) were decreased during VLCD and CONVD relative to baseline in the five participants who lost the most weight (*n* = 5 individuals per time point; mean ± s.e.m.). **c**, Significant differences in bile acid levels between baseline and VCLD phases in these individuals implicate altered bile acid profiles in permissibility to *C. difficile* (*n* = 5 individuals per time point). **a**–**c**, LMM with Tukey's two-sided all-pair comparison. **d**, Working model for the complex interactions between caloric restriction, the gut microbiome, and *C. difficile*. We propose that caloric restriction decreases host production of primary bile acids, including cholic acid, while also lowering total gut microbial colonization and altering the gut microbial community structure. Together, these effects lead to decreased production of the *C. difficile*-inhibitory deoxycholic acid, which allows expansion of *C. difficile*, which, in turn, disrupts host energy balance. Notably, our data also support the existence of *C. difficile*-independent mechanisms for weight loss owing to the restructuring of the gut microbiome following caloric restriction. **e**, Representative culture plate showing presumptive *C. difficile* colonies with characteristic yellow appearance and filamentous edges.

Corresponding author(s): Peter Turnbaugh, Joachim Spranger

Last updated by author(s): Mar 23, 2021

Reporting Summary

Nature Research wishes to improve the reproducibility of the work that we publish. This form provides structure for consistency and transparency in reporting. For further information on Nature Research policies, see our Editorial Policies and the Editorial Policy Checklist.

Statistics

For all statistical analyses, confirm that the following items are present in the figure legend, table legend, main text, or Methods section.

n/a	Confirmed	
☐	☒	The exact sample size (*n*) for each experimental group/condition, given as a discrete number and unit of measurement
☐	☒	A statement on whether measurements were taken from distinct samples or whether the same sample was measured repeatedly
☐	☒	The statistical test(s) used AND whether they are one- or two-sided *Only common tests should be described solely by name; describe more complex techniques in the Methods section.*
☐	☒	A description of all covariates tested
☐	☒	A description of any assumptions or corrections, such as tests of normality and adjustment for multiple comparisons
☐	☒	A full description of the statistical parameters including central tendency (e.g. means) or other basic estimates (e.g. regression coefficient) AND variation (e.g. standard deviation) or associated estimates of uncertainty (e.g. confidence intervals)
☐	☒	For null hypothesis testing, the test statistic (e.g. *F*, *t*, *r*) with confidence intervals, effect sizes, degrees of freedom and *P* value noted *Give P values as exact values whenever suitable.*
☒	☐	For Bayesian analysis, information on the choice of priors and Markov chain Monte Carlo settings
☐	☒	For hierarchical and complex designs, identification of the appropriate level for tests and full reporting of outcomes
☐	☒	Estimates of effect sizes (e.g. Cohen's *d*, Pearson's *r*), indicating how they were calculated

Our web collection on statistics for biologists contains articles on many of the points above.

Software and code

Policy information about availability of computer code

Data collection	No software was use
Data analysis	All statistical and graphical analysis was carried out using R 3.4.0 and R 3.6.0 as described in the methods. A variety of algorithms were used for processing sequencing data including DADA2 v1.1.5 and 1.7.7, Kaiju 1.4.4, and DIAMOND 0.8.25.

For manuscripts utilizing custom algorithms or software that are central to the research but not yet described in published literature, software must be made available to editors and reviewers. We strongly encourage code deposition in a community repository (e.g. GitHub). See the Nature Research guidelines for submitting code & software for further information.

Data

Policy information about availability of data

All manuscripts must include a data availability statement. This statement should provide the following information, where applicable:
- Accession codes, unique identifiers, or web links for publicly available datasets
- A list of figures that have associated raw data
- A description of any restrictions on data availability

Sequencing reads (16S rRNA gene, and shotgun metagenomic) have been deposited in the SRA under BioProject PRJNA412411. The genome of C. difficile JBZPo1 has been deposited under BioProject PRJNA503906. The following public databases were used: The Genome Taxonomy Database (gtdb.ecogenomic.org), DADA2 Taxonomic Training Sets (benjjneb.github.io/dada2/assign.html), CAZy (cazy.org), and KEGG (genome.jp/kegg).

Field-specific reporting

Please select the one below that is the best fit for your research. If you are not sure, read the appropriate sections before making your selection.

☒ Life sciences ☐ Behavioural & social sciences ☐ Ecological, evolutionary & environmental sciences

For a reference copy of the document with all sections, see nature.com/documents/nr-reporting-summary-flat.pdf

Life sciences study design

All studies must disclose on these points even when the disclosure is negative.

Sample size	Sample sizes for the human study were based on the primary study outcomes relating to changes in muscle mass. The microbiome analysis was a secondary and exploratory analysis for which a meaningful power calculation could not be performed a priori. Sample size for gnotobiotic experiments was determined based on feasibility due to housing and breading limitations intrinsic to maintaining animals in a germ-free state.
Data exclusions	No data were excluded.
Replication	Certain gnotobiotic experiments were replicated within and between sites and are reported in Extended Data Fig. 4. A second human cohort replicated the effects of caloric restriction on diversity and taxonomic shifts; however, its results will be reported elsewhere (German Trials Registry DRKS00016536).
Randomization	Humans were block randomized based on BMI and age. Gnotobiotic mice were allocated across treatment groups to balance age, litter, and body weight.
Blinding	Blinding of human intervention study was not possible due to the nature of the intervention (supplying a liquid diet as the sole source of nutrition and restricting caloric intake in subsequent phases)

Reporting for specific materials, systems and methods

We require information from authors about some types of materials, experimental systems and methods used in many studies. Here, indicate whether each material, system or method listed is relevant to your study. If you are not sure if a list item applies to your research, read the appropriate section before selecting a response.

Materials & experimental systems

n/a	Involved in the study
☒	Antibodies
☒	Eukaryotic cell lines
☒	Palaeontology and archaeology
☐	☒ Animals and other organisms
☐	☒ Human research participants
☐	☒ Clinical data
☒	Dual use research of concern

Methods

n/a	Involved in the study
☒	ChIP-seq
☒	Flow cytometry
☒	MRI-based neuroimaging

Animals and other organisms

Policy information about studies involving animals; ARRIVE guidelines recommended for reporting animal research

Laboratory animals	Male C57/BL6J mice aged 10-18 weeks were used for experiments housed in sterile bubble isolators. In all experiments, mice were fed a standard autoclaved chow diet ad libitum (Lab Diet 5021) with free access to water at room temperature of 24 ± 1 °C, room humidity from 30-70%, and a 12/12-h light/dark cycle (7:00 a.m.–7:00 p.m.). Mice were either group housed (Figure 2, Extended Data Fig. 3), or housed individually in duplex cages (all other experiments).
Wild animals	No wild animals were used
Field-collected samples	The study did not involve samples collected from the field.
Ethics oversight	University of California San Francisco Institutional Animal Care and Use Committee, Landesamt fur Gesundheit und Soziales

Note that full information on the approval of the study protocol must also be provided in the manuscript.

Human research participants

Policy information about studies involving human research participants

Population characteristics	Post-menopausal overweight and obese women with ages 58.6±0.9 and 60.1±0.9 mean±sem for the intervention and control groups respectively.
Recruitment	Recruitment was accomplished via official advertisement online and in print. Further recruitment was implemented via our outpatient clinic. Any self-collection bias can be excluded and no study participant was a member of our research group/ clinic. Nonetheless, potential bias remained for recruitment in the endocrine Charité outpatient clinic since patient selection for screening may have been biased by individual evaluation as to whether patients would adhere to the study protocol. Randomization allocation was blinded to the study physicians to avoid selection bias.
Ethics oversight	The study was approved by the Ethik-Kommission der Charité-Universitätsmedizin Berlin.

Note that full information on the approval of the study protocol must also be provided in the manuscript.

Clinical data

Policy information about clinical studies

All manuscripts should comply with the ICMJE guidelines for publication of clinical research and a completed CONSORT checklist must be included with all submissions.

Clinical trial registration	NTC01105143
Study protocol	The study protocol is included as Supplementary Data File 1.
Data collection	Data was collected from March 2012-July 2015 at the ECRC Charite Campus Berlin-Buch.
Outcomes	Microbiome composition was defined as a secondary outcome measure which was measured via 16S rRNA amplicon sequencing and metagenomic sequencing.